Int J Fract (2015) 192:25–45
DOI 10.1007/s10704-014-9983-z

ORIGINAL PAPER

Physically appropriate characterization of fatigue crack propagation rate in elastic–plastic materials using the J-integral concept

W. Ochensberger · O. Kolednik

Received: 5 August 2014 / Accepted: 5 December 2014 / Published online: 19 December 2014

Abstract The current paper discusses the physically correct evaluation of the driving force for fatigue crack propagation in elastic–plastic materials using the J-integral concept. This is important for low-cycle fatigue and for short fatigue cracks, where the conventional stress intensity range (ΔK) concept cannot be applied. Using the configurational force concept, Simha et al. (J Mech Phys Solids 56:2876–2895, 2008) , have derived the J-integral for elastic–plastic materials with incremental theory of plasticity, J^{ep}, which is applicable for cyclic loading and/or for growing cracks, in contrast to the conventional J-integral. The variation of this incremental plasticity J-integral J^{ep} is studied in numerical investigations conducted on two-dimensional C(T)-specimens with long cracks under cyclic Mode I loading. The crack propagates by an increment after each load cycle. The maximum load is varied so that small- and large-scale yielding conditions prevail. Three different load ratios are considered, from pure tension to tension-compression loading. By theoretical considerations and comparisons with the variation of the crack tip opening displacement δ_{t}, it is demonstrated that the cyclic, incremental plasticity J-integral $\Delta J^{\mathrm{ep}}_{\mathrm{actPZ}}$, which is computed for a contour around the active plastic zone of the growing crack, is physically appropriate to characterize the growth rate of fatigue cracks. The validity of the experimental cyclic J-integral, ΔJ^{exp}, proposed by Dowling and Begley (ASTM STP 590:82–103, 1976), is also investigated. The results show that ΔJ^{exp} is correct for the first load cycle, however, not fully appropriate for a growing fatigue crack.

Keywords Configurational force concept · Crack driving force · Cyclic J-integral · Low-cycle fatigue · Fatigue crack growth · Overload effect

W. Ochensberger (✉) · O. Kolednik
Erich Schmid Institute of Materials Science, Austrian Academy of Sciences, Jahnstrasse 12, 8700 Leoben, Austria
e-mail: walter.ochensberger@oeaw.ac.at

W. Ochensberger
Materials Center Leoben Forschung GmbH, Roseggerstrasse 12, 8700 Leoben, Austria

1 Introduction

This paper deals with the physically correct evaluation of the driving force of cyclically loaded, growing cracks in elastic–plastic materials for cases where linear elastic fracture mechanics is not applicable.

The conventional J-integral J^{conv} (Rice 1968a, b), which is commonly applied in the regime of nonlinear fracture mechanics, relies on deformation theory of plasticity, i.e. the elastic–plastic material is treated as being nonlinear elastic. For this reason, J^{conv} suffers from two fundamental problems when it is applied to elastic–plastic materials: (i) J^{conv} is formally not applicable for non-proportional loading conditions (Rice 1968a, b; Anderson 1995), (ii) J^{conv} does not describe the real driving force of a crack in elastic–plastic materials (Rice 1968a, b). In spite of

these problems, Dowling and Begley (1976) proposed the experimental cyclic J-integral ΔJ^{exp} as a parameter characterizing the growth rate $\mathrm{d}a/\mathrm{d}N$ of fatigue cracks for cases where the stress intensity range ΔK is not applicable. Although supported for some materials by experimental data (e.g. Dowling and Begley 1976; Dowling 1976; Lambert et al. 1988; Banks-Sills and Volpert 1991), the applicability of ΔJ^{exp} has remained doubtful due to the lack of its theoretical basis (Suresh 1998).

New insight into this problem has been gained by adopting the concept of configurational forces, which enables the derivation of the J-integral for elastic–plastic materials with incremental theory of plasticity (Simha et al. 2008). This incremental plasticity J-integral J^{ep} has the physical meaning of a real driving force term of a crack in an elastic–plastic material even under strongly non-proportional loading conditions, however it is path dependent (Simha et al. 2008). Kolednik et al. (2014) studied this path dependence and demonstrated the usefulness of J^{ep} for stationary and growing cracks under monotonic loading conditions. In a very recent study, Ochensberger and Kolednik (2014) have investigated the application of J^{ep} for stationary cracks in elastic–plastic materials that are cyclically loaded, and it has been shown that the experimental cyclic J-integral ΔJ^{exp} is, in principle, correct, if certain conditions are observed.

The current paper complements the study of Ochensberger and Kolednik (2014) by considering *growing* cracks in elastic–plastic, cyclically loaded materials. It will be demonstrated that important differences occur compared to the case of a stationary crack. The paper shall provide a new basis for the application of the J-integral concept for characterizing the crack growth rate in fatigue.

The next section briefly reviews the incremental plasticity J-integral J^{ep} and the findings of the papers by Kolednik et al. (2014) and Ochensberger and Kolednik (2014) that are necessary for the understanding of the current paper. Readers who are already familiar with the topic may continue reading at the last paragraph in Sect. 2.

2 Incremental plasticity J-integral J^{ep} and crack driving force

Configurational forces are thermodynamic driving forces on defects in materials (Maugin 1995; Gurtin 1995, 2000; Kienzler and Herrmann 2000). The application of the configurational force concept for studying fracture mechanics problems has gained increasing research interest, see e.g. Simha et al. (2003; 2005), Nguyen et al. (2005), Özenç et al. (2014), Sistaninia and Kolednik (2014), Kolednik et al. (2014) and the according references in Sect. 2 therein. The concept rests on the notion of the second-rank configurational stress tensor, which is defined in the form, $\mathbf{C} = \phi\mathbf{I} - \mathbf{F}^{\mathrm{T}}\mathbf{S}$ (Eshelby 1951, 1970).[1] The parameter ϕ denotes the strain energy density, $\mathbf{I}$ the identity tensor, $\mathbf{F}^{\mathrm{T}}$ the transposed of the deformation gradient tensor $\mathbf{F}$, and $\mathbf{S}$ the 1st Piola-Kirchhoff stress. A configurational force $\mathbf{f}$ in a body is associated with the divergence of the configurational stress tensor,

$$\mathbf{f} = -\nabla \cdot \mathbf{C} = -\nabla \cdot \left(\phi\mathbf{I} - \mathbf{F}^{\mathrm{T}}\mathbf{S}\right). \tag{1}$$

The vector $\mathbf{f}$ gives the magnitude and direction of the thermodynamic driving force acting on the defect.

2.1 Configurational forces and J-integrals for elastic–plastic materials

A literature review on the application of configurational force concept for the prediction of the behavior of cracks has been given in Kolednik et al. (2014) and shall not be repeated here. Figure 1a shows a sketch of a homogeneous body $\mathcal{B}$ containing a crack with length a_0 and a unit vector in the nominal crack growth direction $\mathbf{e}$. The configurational force concept allows the derivation of the J-integral. The scalar, near-tip J-integral J_{tip} is related to the configurational force vector emanating from the crack tip, $\mathbf{f}_{\mathrm{tip}}$, in the form (see e.g. Simha et al. 2003),

$$J_{\mathrm{tip}} = \mathbf{e} \cdot \mathbf{J}_{\mathrm{tip}} = \mathbf{e} \cdot \left(-\mathbf{f}_{\mathrm{tip}}\right) = \mathbf{e} \cdot \lim_{r \to 0} \int_{\Gamma_r} \mathbf{C}\,\mathbf{n}\,\mathrm{d}s, \tag{2}$$

where Γ_r is a contour drawn from the lower to the upper crack surface in counterclockwise direction at a distance r around the crack tip; $\mathbf{n}$ is the outward unit normal vector to the contour Γ, and $\mathrm{d}s$ is an increment of the integration path. The scalar J-integral J_{tip} of Eq. (2) is the projection of the near-tip J-integral vector $\mathbf{J}_{\mathrm{tip}}$ into the nominal crack growth direction $\mathbf{e}$. The

[1] For the mathematical expressions in this paper the direct (coordinate-free) notation is used as in Gurtin (2000). The notation is specified in Ochensberger and Kolednik (2014).

J-integral along an arbitrary contour Γ can be evaluated from the relation,

$$J = \mathbf{e}\cdot\mathbf{J} = \mathbf{e}\cdot\int_{\Gamma}\mathbf{C}\,\mathbf{n}\,\mathrm{d}s = \mathbf{e}\cdot\int_{\Gamma}\left(\phi\mathbf{I}-\mathbf{F}^{\mathrm{T}}\mathbf{S}\right)\mathbf{n}\,\mathrm{d}s$$
$$= J_{\mathrm{tip}} - \mathbf{e}\cdot\int_{\mathcal{D}}\mathbf{f}\,\mathrm{d}A, \tag{3}$$

where $\mathcal{D}$ denotes the area bounded by Γ, but excluding the crack tip. Note that Eqs. (2) and (3) do not rely on constitutive equations of the material.

We assume that body $\mathcal{B}$ is homogeneous and consists of elastic–plastic material. Then we can distinguish between two different types of J-integral, the conventional J-integral J^{conv}, which presumes deformation theory of plasticity (see e.g. Simha et al. 2003), and the incremental plasticity J-integral J^{ep} for materials with incremental theory of plasticity (Simha et al. 2008),

$$J^{\mathrm{conv}} = J^{\mathrm{conv}}_{\mathrm{tip}} + \mathbf{e}\cdot\int_{\mathcal{D}}\nabla\cdot\left(\phi\mathbf{I}-\mathbf{F}^{\mathrm{T}}\mathbf{S}\right)\mathrm{d}A$$
$$= J^{\mathrm{conv}}_{\mathrm{tip}} - \mathbf{e}\cdot\int_{\mathcal{D}}\mathbf{f}^{\mathrm{def.pl}}\mathrm{d}A, \tag{4}$$

$$J^{\mathrm{ep}} = J^{\mathrm{ep}}_{\mathrm{tip}} + \mathbf{e}\cdot\int_{\mathcal{D}}\nabla\cdot\left(\phi_{\mathrm{e}}\mathbf{I}-\mathbf{F}^{\mathrm{T}}\mathbf{S}\right)\mathrm{d}A$$
$$= J^{\mathrm{ep}}_{\mathrm{tip}} - \mathbf{e}\cdot\int_{\mathcal{D}}\mathbf{f}^{\mathrm{ep}}\mathrm{d}A. \tag{5}$$

The difference between J^{conv} and J^{ep} appears in the substitution of the strain energy density ϕ. For deformation plasticity, the total strain energy density ϕ is inserted as for a nonlinear elastic material, whereas for incremental plasticity only the elastic part of the strain energy density ϕ_{e} is inserted, see Fig. 1c. From Eqs. (4) and (5), or by inserting either ϕ or ϕ_{e} into Eq. (1), it is clear that also two different types of configurational force exist, the deformation plasticity configurational force $\mathbf{f}^{\mathrm{def.pl}}$ and the elastic–plastic configurational force $\mathbf{f}^{\mathrm{ep}}$.

If the body $\mathcal{B}$ deforms only elastically, there exists no difference between $\mathbf{f}^{\mathrm{def.pl}}$ and $\mathbf{f}^{\mathrm{ep}}$, or between J^{conv} and J^{ep}. The bulk configurational force $\mathbf{f}$ vanishes, and configurational forces appear only at the crack tip, $\mathbf{f}_{\mathrm{tip}}$, and at the external boundary $\partial\mathcal{B}$ (Fischer et al. 2012). Therefore, the J-integral is path-independent, see the right-hand side extension of Eq. (4).

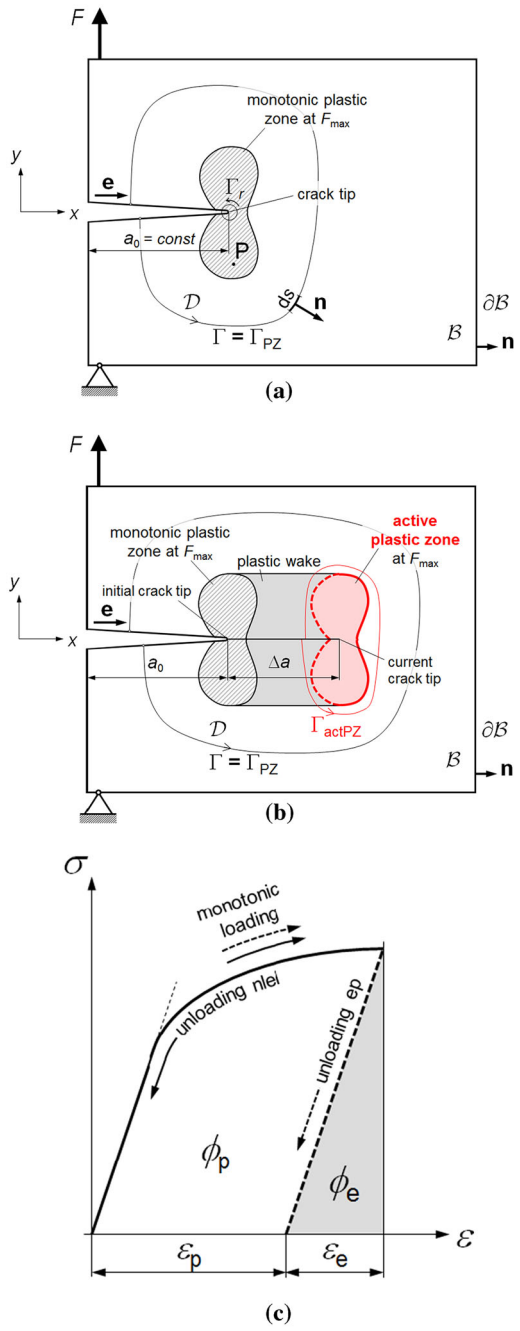

Fig. 1 **a** Homogeneous elastic–plastic body $\mathcal{B}$ with a long, stationary crack. The contour Γ_{PZ} encloses the crack tip plastic zone. **b** Body $\mathcal{B}$ after crack extension Δa. The contour Γ_{actPZ} encloses the active plastic zone of the current crack tip, whereas the contour Γ_{PZ} encloses the entire crack tip plastic zone, including the plastic wake. **c** Stress–strain ($\sigma-\varepsilon$) curve for point P in the plastic zone. Only the elastic part of the strain energy density ϕ_{e} is reversible. The total strain energy density $\phi = \phi_{\mathrm{e}} + \phi_{\mathrm{p}}$ would be recoverable in a comparable nonlinear elastic material with the identical $\sigma-\varepsilon$-curve

If body $\mathcal{B}$ is also plastically deformed, bulk configurational forces $\mathbf{f}^{\mathrm{ep}}$ are induced in the plastically deformed regions of the body and, according to the right-hand side extension of Eq. (5), the incremental plasticity J-integral J^{ep} becomes path-dependent. The bulk configurational force $\mathbf{f}^{\mathrm{ep}}$ at a material point in the elastic–plastic body evolves proportional to the gradient of the plastic component of the deformation gradient (Simha et al. 2008),

$$\mathbf{f}^{\mathrm{ep}} = \left(\mathbf{F}^{\mathrm{e}}\right)^{\mathrm{T}} \mathbf{S} : \frac{\partial \mathbf{F}^{\mathrm{p}}}{\partial \mathbf{X}}. \tag{6}$$

In Eq. (6), $\mathbf{F}^{\mathrm{e}}$ and $\mathbf{F}^{\mathrm{p}}$ are the elastic and plastic components of the deformation gradient tensor $\mathbf{F}$, and $\partial \mathbf{F}^{\mathrm{p}}/\partial \mathbf{X}$ is the gradient of $\mathbf{F}^{\mathrm{p}}$ with respect to the unloaded reference coordinate system.

Performing a numerical cyclic tensile test, Kolednik et al. (2014) have demonstrated the problem of idealizing elastic–plastic materials with deformation theory of plasticity: artificial bulk configurational forces $\mathbf{f}^{\mathrm{def.pl}}$ emerge on positions with a gradient in plastic strain as soon as non-proportional loading occurs. These bulk configurational forces do not have a physical background and lead to an artificial path dependence of J^{conv}, compare Eq. (4); see also Brocks et al. (2003) or, e.g., in Kuna (2008).

A big advantage of the incremental plasticity J-integral J^{ep} is that it has the physical meaning of a true driving force term in elastic–plastic materials even for non-proportional loading conditions, such as a growing crack or a cyclically loaded crack, while, on the contrary, the conventional J-integral J^{conv} possesses the well-known restrictions outlined in the Introduction.

2.2 Path dependence of J^{ep} and driving force for cracks under monotonic loading

The path dependence of the incremental plasticity J-integral J^{ep} for stationary and growing cracks in monotonically loaded elastic–plastic materials has been investigated in Kolednik et al. (2014). The investigation showed that for a stationary crack, the J-integral for a contour enclosing the entire crack tip plastic zone $J^{\mathrm{ep}}_{\mathrm{PZ}}$, Fig. 1a, should be taken as parameter characterizing the driving force. Crack extension occurs, if $J^{\mathrm{ep}}_{\mathrm{PZ}}$ is equal or larger than the crack growth resistance.

The incremental plasticity J-integral for a contour enclosing the crack tip plastic zone $J^{\mathrm{ep}}_{\mathrm{PZ}}$ has the physical meaning of the driving force for the combined movement of the crack tip and the crack tip plastic zone. From a comparison of Fig. 1a, b it becomes clear that it is impossible for a crack to grow in an elastic–plastic material without the simultaneous movement of the surrounding plastic zone. Thus, the near-tip J-integral $J^{\mathrm{ep}}_{\mathrm{tip}}$, which is the driving force for the translational movement of the crack tip alone, is meaningless for the assessment of crack extension. The numerical results in Kolednik et al. (2014) suggest that the magnitude of the incremental plasticity near-tip J-integral is zero, $J^{\mathrm{ep}}_{\mathrm{tip}} = 0$, for both a stationary and a growing crack under monotonic loading. As noted already in classical papers, e.g. Rice and Johnson (1970) or Rice (1979), also the conventional, deformation plasticity near-tip J-integral is zero, $J^{\mathrm{conv}}_{\mathrm{tip}} = 0$, for stationary and growing cracks under monotonic loading.

For a contour around the crack tip plastic zone, the conventional J-integral $J^{\mathrm{conv}}_{\mathrm{PZ}}$ is identical to the incremental plasticity J-integral $J^{\mathrm{ep}}_{\mathrm{PZ}}$,

$$J^{\mathrm{ep}}_{\mathrm{PZ}} = J^{\mathrm{conv}}_{\mathrm{PZ}}. \tag{7}$$

The requirement for this equality is that the crack tip plastic zone is completely surrounded by material that is only elastically deformed. In this case there is no difference in the formulation between deformation- and incremental plasticity, see middle term in Eq. (3).

Notice that a relation similar to Eq. (7) for the far-field J-integrals, $J^{\mathrm{ep}}_{\mathrm{far}} = J^{\mathrm{conv}}_{\mathrm{far}}$, only exists, if no part of the outer boundary of the specimen is plastically deformed. A back-face plasticity region appears in case of large-scale yielding (lsy) conditions, compare Fig. 4b. Configurational forces $\mathbf{f}^{\mathrm{ep}}$ with a positive component in x-direction are induced in the back-face plasticity region so that J^{ep} decreases and $J^{\mathrm{ep}}_{\mathrm{far}} < J^{\mathrm{ep}}_{\mathrm{PZ}}$, compare Eq. (5). On the contrary, the conventional J-integral remains constant, $J^{\mathrm{conv}}_{\mathrm{far}} = J^{\mathrm{conv}}_{\mathrm{PZ}}$, since proportional loading conditions prevail. It is well known that for a stationary crack the conventional J-integral J^{conv} equals the experimental J-integral J^{exp}, which is determined from the load–displacement curve (Rice et al. 1973; Kolednik 1991). Therefore, the incremental plasticity J-integral for a contour around the crack tip plastic zone $J^{\mathrm{ep}}_{\mathrm{PZ}}$ equals the experimental J-integral for a stationary crack, $J^{\mathrm{ep}}_{\mathrm{PZ}} = J^{\mathrm{conv}}_{\mathrm{PZ}} = J^{\mathrm{conv}}_{\mathrm{far}} = J^{\mathrm{exp}}$. This means that both the conventional and the experimental J-integral give the correct driving force for the initiation of crack growth.

For a continuously growing crack at constant load, the J-integral J^{ep}_{actPZ} for a contour Γ_{actPZ} around the *active* plastic zone of the moving crack tip, Fig. 1b, is the physically correct crack driving force parameter (Kolednik et al. 2014). Here, the contour Γ_{PZ} encloses the initial plastic zone of the stationary crack, the plastically deformed regions along the crack flanks (plastic wake), and the active plastic zone around the current crack tip. Since the contour Γ_{PZ} goes only through elastic deformed regions, Eq. (7) is still valid. However, note that $J^{ep}_{actPZ} \neq J^{conv}_{actPZ}$, since the contour Γ_{actPZ} crosses the plastic wake along the crack flanks (Fig. 1b). It should be mentioned that the experimental J-integral J^{exp} does, in general, not reflect the driving force for a growing crack, $J^{ep}_{actPZ} \neq J^{exp}$; see Kolednik (1991; 1993) and Turner and Kolednik (1994). This means that neither the conventional nor the experimental J-integral give the correct driving force for a continuously growing crack under monotonic loading.

2.3 Driving force for cyclically loaded, stationary cracks in elastic–plastic materials

The characteristic properties of the incremental plasticity J-integral J^{ep} under cyclic loading conditions, but for a *stationary* crack, have recently been presented in Ochensberger and Kolednik (2014). The path-dependence of J^{ep} was investigated for various, positive and negative, load ratios $R = F_{min}/F_{max}$ under lsy-conditions. It has been shown that negative J^{ep}-values can appear during the unloading stages on contours close to the crack tip; they originate from compressive residual stresses caused by reverse plasticity within the crack tip plastic zone.

The incremental plasticity J-integral for a contour enclosing the crack tip plastic zone J^{ep}_{PZ} also characterizes the driving force of a crack in an elastic–plastic material, which is monotonically loaded after a cyclic pre-deformation. It is clear that $J^{ep}_{PZ} = J^{conv}_{PZ}$, since Eq. (7) is valid also for cyclic loading conditions, as long as the crack tip plastic zone is surrounded by elastically deformed material.

In the fatigue of metals and alloys, the magnitude of the crack driving force at the maximum load $J^{ep}_{PZ,max}$ is considerably smaller than the crack growth resistance, so that the crack cannot extend at F_{max} = constant. Driving force terms for fatigue crack growth have been introduced, which should allow the prediction of the crack propagation rate of a fatigue crack (e.g. see Suresh 1998). Note that these terms are not necessarily real driving force terms in the thermodynamic sense. The stress intensity range ΔK (Paris et al. 1961; Paris and Erdogan 1963) or the effective stress intensity range ΔK_{eff} (Elber 1970, 1971) are used, if linear elastic fracture mechanics is applicable. For the regime of elastic–plastic fracture mechanics, Dowling and Begley (1976) proposed the application of the experimental cyclic J-integral ΔJ^{exp}, which is determined from a single loading or unloading branch of the load–displacement ($F - v$) curve, similar to J^{exp} for monotonic loading. For deeply notched bend- and C(T)-specimens, ΔJ^{exp} is given by the relation

$$\Delta J^{exp} = \frac{\eta \Delta A}{bB}, \tag{8}$$

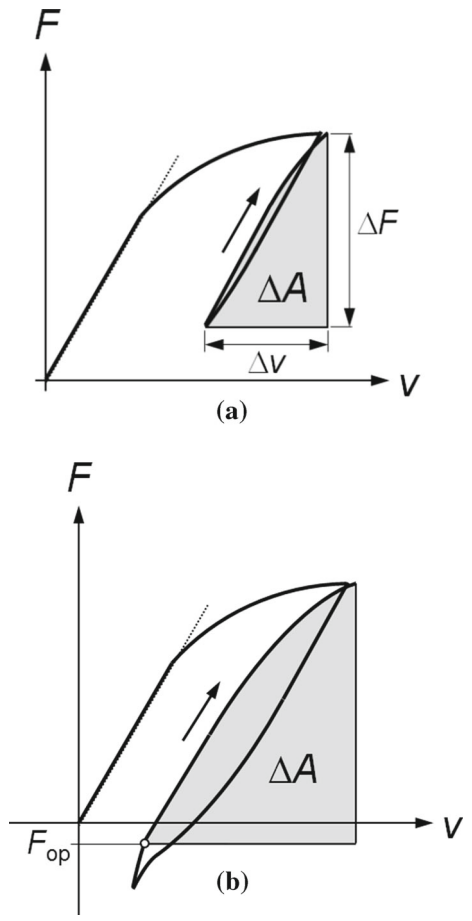

Fig. 2 To the determination of the experimental cyclic J-integral ΔJ^{exp} for a C(T) or deeply notched bend specimen from the area ΔA below a single loading branch of the load–displacement ($F - v$) curve, **a** for load ratio $R > 0$ without crack closure, **b** for $R < 0$. The load F_{op} denotes the point of crack opening

where ΔA is the area below a single loading branch of the $F - v$-curve (Fig. 2a), $b = W - a$ is the ligament length, with W as the specimen width and a as the crack length, and B is the specimen thickness. The geometry factor $\eta(a/W)$ depends on the specimen type (see also ESIS P2-92 1992 or ASTM E1820 2005). In spite of empirical results showing that ΔJ^{exp} correlates to $\mathrm{d}a/\mathrm{d}N$ for specific materials under certain cyclic loading conditions (e.g. Dowling and Begley 1976; Dowling 1976; Lambert et al. 1988; Banks-Sills and Volpert 1991), the general applicability of ΔJ^{exp} remained doubtful due to the lack of theoretical basis (Anderson 1995; Suresh 1998).

Ochensberger and Kolednik (2014) have shown that the incremental plasticity cyclic J-integral for a contour around the crack tip plastic zone, $\Delta J^{\mathrm{ep}}_{\mathrm{PZ}}$, is a physically appropriate parameter for characterizing the driving force for a cyclically loaded, stationary crack. The parameter $\Delta J^{\mathrm{ep}}_{\mathrm{PZ}}$ should be evaluated by the relation,

$$\Delta J^{\mathrm{ep}}_{\mathrm{PZ}} = J^{\mathrm{ep}}_{\mathrm{PZ,max}} + J^{\mathrm{ep}}_{\mathrm{PZ,\,min}} - 2\sqrt{J^{\mathrm{ep}}_{\mathrm{PZ,\,max}} J^{\mathrm{ep}}_{\mathrm{PZ,\,min}}}. \quad (9)$$

Here, $J^{\mathrm{ep}}_{\mathrm{PZ,max}}$ and $J^{\mathrm{ep}}_{\mathrm{PZ,min}}$ denote the maximum and minimum $J^{\mathrm{ep}}_{\mathrm{PZ}}$-values achieved in a single load cycle. It should be mentioned that the magnitude of $\Delta J^{\mathrm{ep}}_{\mathrm{PZ}}$ is, due to the square root term in Eq. (9), very sensitive to small values of $J^{\mathrm{ep}}_{\mathrm{PZ,min}}$. This fact is especially important for small positive load ratios. For a stationary crack, negative load ratios gave minimum $J^{\mathrm{ep}}_{\mathrm{PZ}}$-values of exactly zero, $J^{\mathrm{ep}}_{\mathrm{PZ,min}} = 0$, leading to $\Delta J^{\mathrm{ep}}_{\mathrm{PZ}} = J^{\mathrm{ep}}_{\mathrm{PZ,max}}$ (Ochensberger and Kolednik 2014).

The application of Eq. (9) for the correct calculation of the cyclic J-integral can be demonstrated by comparison with the cyclic crack tip opening displacement $\Delta\delta_{\mathrm{t}}$ (Ochensberger and Kolednik 2014). In a very recent study, Metzger et al. (2014) demonstrated the correlation between the conventional cyclic J-integral (Lamba 1975; Wüthrich 1982; Tanaka 1983) and $\Delta\delta_{\mathrm{t}}$. Note that the conventional cyclic J-integral used in Metzger et al. (2014) is, in principle, equal to the expression in Eq. (9), see Appendix in Ochensberger and Kolednik (2014) for details.

If the crack tip plastic zone is completely surrounded by elastically deformed material, Eq. (7) applies for both the J^{ep}-values at maximum and minimum load. Therefore, the incremental plasticity and deformation plasticity cyclic J-integrals for a contour around the crack tip plastic zone must be equal,

$$\Delta J^{\mathrm{ep}}_{\mathrm{PZ}} = \Delta J^{\mathrm{conv}}_{\mathrm{PZ}} = \Delta J^{\mathrm{exp}}. \quad (10)$$

The right-hand side extension of Eq. (10) results from Ochensberger and Kolednik (2014), who have shown that the experimental cyclic J-integral ΔJ^{exp} reflects the magnitude of $\Delta J^{\mathrm{ep}}_{\mathrm{PZ}}$, provided that in cases of crack closure a correct procedure is applied for the determination of the area ΔA in Eq. (8). The conventionally applied procedure via the determination of the closure- or opening loads, F_{cl} and F_{op} (Fig. 2b), as proposed by Dowling and Begley (1976), can lead to inaccurate results, see also Sect. 5.2 below.

The results of Ochensberger and Kolednik (2014) demonstrate that the experimental cyclic J-integral ΔJ^{exp} proposed by Dowling and Begley (1976) is, in principle, a physically appropriate driving force parameter for a cyclically loaded specimen. It should be noted, however, that this investigation has been conducted for a stationary crack. Therefore, the question remains to be solved whether these findings are applicable also in the case where the crack grows under cyclic loading, as it occurs in fatigue crack growth.

We consider in the current paper cyclic loading *with* crack extension. It will be demonstrated in this paper that important differences appear between a stationary and a growing crack, although the crack growth rate per load cycle is small.

3 Numerical modeling and computational aspects

For the numerical investigations the same procedure is applied as in Ochensberger and Kolednik (2014). The simulations are performed using the finite element (FE) program ABAQUS (see http://www.simulia.com/products/abaqus_fea.html). A two-dimensional C(T)-specimen (ASTM E1820, 2005) is modeled with a straight crack in horizontal x-direction, Fig. 3a. The specimen dimensions are: width $W = 50$ mm, height $H = 60$ mm, nominal thickness $B = 25$ mm, and initial crack length $a_0 = 25$ mm. The specimen is subjected to cyclic Mode I loading by prescribing the load F at the load application point. Plane strain conditions are assumed.

The specimen consists of homogeneous, isotropic, elastic–ideally plastic material with Young's modulus $E = 200$ GPa, Poisson's ratio $\nu = 0.3$, and yield strength $\sigma_{\mathrm{y}} = 270$ MPa. A small strip near the left boundary of the specimen is adopted as linear elastic, with Young's modulus $E = 200$ GPa and Poisson's ratio $\nu = 0.3$. This is done to prevent large plastic

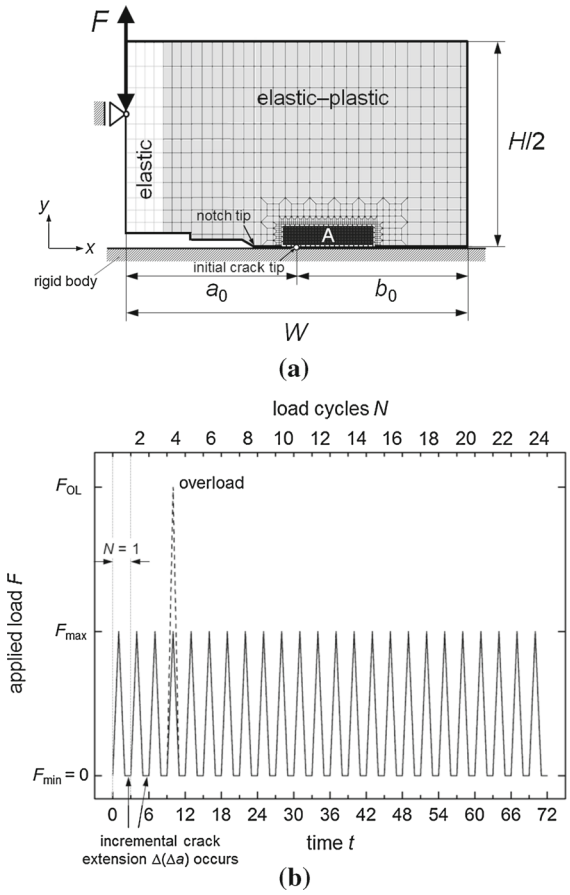

Fig. 3 **a** Model of the C(T)-specimen with boundary conditions. **b** Applied load F versus time t for a load ratio $R = 0$; the increment of crack extension per load cycle $\Delta(\Delta a)$ is two element lengths. Apart from the cases with constant loads, an additional study is conducted for a single tensile overload F_{OL}, applied during the fourth load cycle

deformation at the load application point. Note that this does not cause any problems, since the plastic zone does not approach the elastic region.

Half of the specimen is discretized (Fig. 3a). The mesh consists of bilinear 4-node continuum elements. The inner region A, where the crack propagates, has a dimension of $13.5 \times 3.0\,\mathrm{mm}^2$; it is filled with elements of equal size. If not specified otherwise, the element size is $m = 0.1$ mm. Geometric nonlinearity is applied to consider large deformations around the crack tip. Crack flank contact without friction is modeled; a rigid body serves as counterpart to the upper half of the specimen. The nodes on the plane $y = 0$, except the nodes on the crack flank, are locked in y-direction, but unlocked in x-direction.

The loading steps are shown in Fig. 3b. Each load cycle N can be divided into three steps. In the first step, finished at time $t = 3N - 2$ with $N \in \mathbb{N}$, the specimen is loaded to maximum load $F_{\max}$. In the second step, finished at $t = 3N - 1$, the specimen is unloaded to minimum load $F_{\min}$. The crack length is held fixed during the loading and unloading stages. In the third step, finished at $t = 3N$, the crack extends by an increment at the minimum load $F_{\min}$. We refer to Solanki et al. (2004) regarding the preferred load level for incremental crack extension. Incremental crack extension is modeled by adopting the node release technique (Ohji et al. 1975; Newman 1976). Hereby initially bonded nodes on the plane $y = 0$ are released according to a pre-defined crack length function of time (see also Kuna 2008). Two elements are chosen as crack extension increment per load cycle, $\Delta(\Delta a) = 2m$. The number of applied load cycles is $N = 24$; the total crack advance is $\Delta a = \sum_{i=1}^{N} \Delta(\Delta a)_i = 4.8$ mm.

The maximum load is varied so that we get small-scale yielding (ssy) and large-scale yielding (lsy) conditions at $F_{\max} = 12.5\,\mathrm{kN}$ and $F_{\max} = 27\,\mathrm{kN}$, respectively (Fig. 4a, b). Large-scale yielding is assumed to start with the onset of plasticity at the back face of the specimen (Fig. 4b). Three load ratios are considered, $R = 0$ (zero-tension loading, Fig. 3b), $R = 0.5$ (pure tension), and $R = -1$ (tension-compression).

The FE stress and strain analyses are in all cases performed using the incremental plasticity model provided by ABAQUS. Subsequently, the configurational forces are evaluated by a self-written post-processing routine, which is based on the papers by Müller et al. (2002; 2004) and Denzer et al. (2003). Deformation plasticity and incremental plasticity are alternatively applied for this post-processing in order to calculate at each node the deformation- and incremental plasticity configurational force, $\mathbf{f}^{\mathrm{def.pl}}$ and $\mathbf{f}^{\mathrm{ep}}$, by inserting either ϕ and ϕ_{e} into Eq. (1).

The scalar J-integral for an arbitrary contour Γ is calculated by a summation of the configurational forces over all nodes within the area $\mathcal{D}$ bounded by Γ, including the crack tip node, compare Eqs. (4) and (5). The J-integrals for deformation plasticity and incremental plasticity, J^{conv} and J^{ep}, are given by

$$J_{\Gamma}^{\mathrm{conv}} = \sum_{n \in \mathcal{D} \cup \mathrm{tip}} - \left(\mathbf{e} \cdot \mathbf{f}^{\mathrm{def.pl}} \right) \Delta A_n, \tag{11}$$

$$J_{\Gamma}^{\mathrm{ep}} = \sum_{n \in \mathcal{D} \cup \mathrm{tip}} - \left(\mathbf{e} \cdot \mathbf{f}^{\mathrm{ep}} \right) \Delta A_n. \tag{12}$$

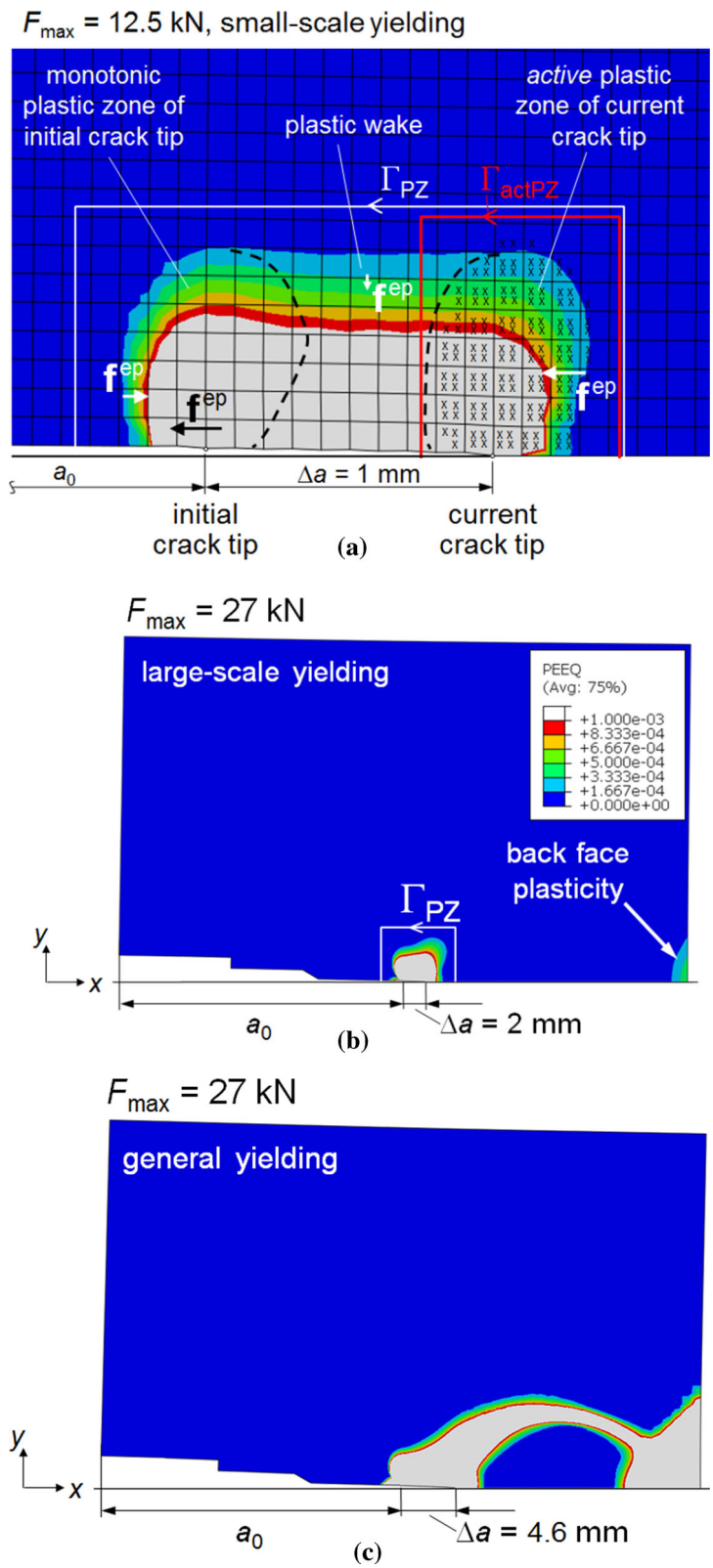

Fig. 4 Maps of the equivalent plastic strain ε_{eq}^{p} at an applied load of **a** $F_{max} = 12.5$ kN (small-scale yielding conditions), **b** $F_{max} = 27$ kN (large-scale yielding, i.e. after onset of back face plasticity), and **c** at $F_{max} = 27$ kN and $\Delta a = 4.6$ mm (general yielding). In **a** the configuration after $\Delta a = 1$ mm crack extension is depicted, when the active plastic zone has completely left the monotonic plastic zone of the initial crack tip; the *plastic zone shapes* are marked with *dashed lines*. Γ_{PZ} and Γ_{actPZ} denote the contours around the entire and the active plastic zone, respectively. Directions of the bulk configurational force $\mathbf{f}^{ep}$ are schematically indicated

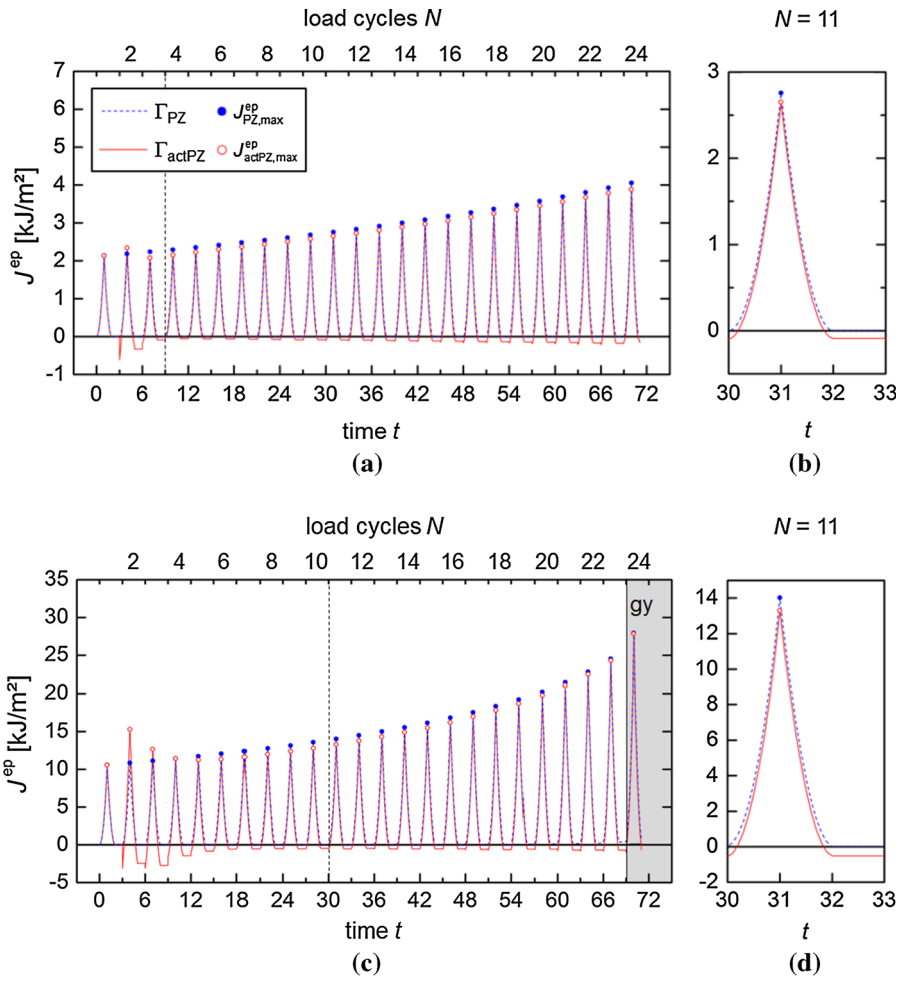

Fig. 5 Incremental plasticity J-integrals around the crack tip plastic zone, J^{ep}_{PZ}, and around the active plastic zone, J^{ep}_{actPZ}, versus time t for **a** small-scale yielding; **c** large-scale yielding, turning to general yielding after show $t = 69$, $\Delta a = 4.6$ mm. **b**, **d** show a detail of the 11th load cycle. The values reached at maximum load, $J^{ep}_{PZ,max}$ and $J^{ep}_{actPZ,max}$, are marked with *full* and *open dots*, respectively. The *vertical dashed lines* indicate when the active plastic zones leave the initial crack tip plastic zones

The parameter ΔA_n denotes the element area corresponding to a specific node n.

Important are the computation of J-integrals around the crack tip plastic zone J_{PZ} and around the active plastic zone J_{actPZ}, see Fig. 1b. The shape of the active plastic zone is obtained by observation of currently yielding integration points, i.e. when the plastic strain $\boldsymbol{\varepsilon}^p$ changes during a loading sequence. An example is presented in Fig. 4a; currently yielding integration points are marked by x-symbols. The integration path Γ_{actPZ} is chosen so that it includes all marked integration points at maximum load F_{max}. It should be noted that the magnitude of the integration path is held fixed for a specific loading and unloading sequence, i.e. Γ_{actPZ} does not vary with increasing or decreasing load.

In addition to the J-integrals derived from configurational forces, J^{conv} and J^{ep}, the conventional computational J-integral of ABAQUS J^{VCE}, which is based on the virtual crack extension method developed by Parks (1977), is also computed. Note that J^{VCE} implicitly relies on deformation plasticity, when applied to elastic–plastic materials.

4 Incremental plasticity J-integral J^{ep} for crack extension under cyclic loading

4.1 Characteristic incremental plasticity J-integral terms, J^{ep}_{PZ} and J^{ep}_{actPZ}

Figure 5a, c present, for a load ratio $R = 0$, the variations of the incremental plasticity J-integrals around the crack tip plastic zone, J^{ep}_{PZ}, and around the active plastic zone, J^{ep}_{actPZ}, under ssy- and lsy-conditions, i.e. $F_{max} = 12.5$ kN and $F_{max} = 27$ kN, respectively. Shown are $N = 24$ load cycles; Fig. 5b, d show in more detail the 11th load cycle. The J^{ep}-values reached at

Table 1 Values of the incremental plasticity J-integrals around the crack tip plastic zone, J^{ep}_{PZ}, and around the active plastic zone, J^{ep}_{actPZ}, for small-scale yielding conditions

R	N	Δa (mm)	$J^{ep}_{PZ,max}$ (kJ/m^2)	$J^{ep}_{PZ,min}$	$J^{ep}_{actPZ,max}$	$J^{ep}_{actPZ,min}$	$\Delta^{JactPZ,max}_{JPZ,max}$ (%)	ΔJ^{ep}_{PZ} (kJ/m^2)	ΔJ^{ep}_{actPZ}	ΔJ^{exp}	$\Delta^{\Delta JactPZ}_{\Delta JPZ}$ (%)
0	1	0	2.132	0.000	2.132	0.000	0.00	–	–	2.082	–
0	2	0.2	2.184	8.0e−5	2.341	−0.621	6.71	2.157	2.341	2.121	7.86
0	6	1	2.415	2.0e−4	2.280	−0.062	−5.92	2.372	2.280	2.358	−4.04
0	11	2	2.759	2.8e−4	2.653	−0.087	−4.00	2.703	2.653	2.705	−1.88
0	16	3	3.177	3.8e−4	3.059	−0.119	−3.86	3.108	3.059	3.119	−1.60
0	21	4	3.691	5.6e−4	3.558	−0.134	−3.74	3.600	3.558	3.621	−1.18
0	24	4.6	4.056	7.1e−4	3.882	−0.156	−4.48	3.949	3.882	3.973	−1.73
0.5	1	0	2.132	0.000	2.132	0.540	0.00	–	–	2.082	–
0.5	2	0.2	2.183	0.540	2.264	0.444	3.58	0.552	0.703	0.549	21.5
0.5	6	1	2.414	0.612	2.279	0.576	−5.92	0.595	0.564	0.595	−5.50
0.5	11	2	2.755	0.700	2.633	0.604	−4.63	0.678	0.715	0.683	5.17
0.5	16	3	3.170	0.809	2.948	0.609	−7.53	0.776	0.877	0.790	11.5
0.5	21	4	3.682	0.943	3.417	0.698	−7.76	0.898	1.026	0.918	12.5
0.5	24	4.6	4.046	1.039	3.748	0.762	−7.95	0.984	1.130	1.009	12.9
−1	1	0	2.132	0.000	2.132	5.7e−6	0.00	–	–	2.082	–
−1	2	0.2	2.184	5.7e−6	2.352	−0.625	7.23	2.177	2.352	2.129	7.44
−1	6	1	2.415	1.6e−4	2.300	−0.066	−5.00	2.376	2.300	2.359	−3.30
−1	11	2	2.760	2.0e−4	2.654	−0.090	−3.99	2.713	2.654	2.705	−2.22
−1	16	3	3.178	2.8e−4	3.061	−0.120	−3.82	3.119	3.061	3.119	−1.89
−1	21	4	3.692	4.4e−4	3.560	−0.122	−3.71	3.612	3.560	3.621	−1.46
−1	24	4.6	4.058	5.6e−4	3.883	−0.156	−4.51	3.962	3.883	3.974	−2.03

The parameter R denotes the load ratio, N the load cycle number, and Δa the crack extension. The indices "max" and "min" denote maximum and minimum values during a load cycle. The values of the experimental cyclic J-integral ΔJ^{exp} are shown for comparison. Columns with Δ^i_j denote the relative difference between two values i, j

maximum load F_{max} are marked with full (for $J^{ep}_{PZ,max}$) and open (for $J^{ep}_{actPZ,max}$) dots.

It is seen from Fig. 5 that, due to the crack extension after each load cycle, the J^{ep}-values at maximum load, $J^{ep}_{PZ,max}$ and $J^{ep}_{actPZ,max}$, continuously increase, whereas the values taken at minimum load, $J^{ep}_{PZ,min}$ and $J^{ep}_{actPZ,min}$, remain approximately constant. While J^{ep}_{PZ} shows a regular behavior, with values very close to zero at F_{min}, the J^{ep}_{actPZ}-curve exhibits some irregularities during the first load cycles. The J^{ep}_{actPZ}-curve appears shifted downwards compared to the J^{ep}_{PZ}-curve.

The values of J^{ep}_{actPZ} and J^{ep}_{PZ} are equal for the first loading and unloading cycle, since crack extension has not occurred yet. With the first crack extension step, time $t > 2$, the active plastic zone starts to leave the plastic zone of the initial crack tip, and J^{ep}_{actPZ} differs from J^{ep}_{PZ}. The active plastic zone has completely left the initial plastic zone after a crack extension of $\Delta a = 0.6$ and 2 mm, $N = 4$ and 11, for ssy- and lsy-conditions, respectively. This is indicated by a vertical dashed line in Fig. 5a, c. It is seen that the irregularities of the J^{ep}_{actPZ}-curve occur before this line; e.g. especially high $J^{ep}_{actPZ,max}$-values appear during $N = 2$, followed by especially low $J^{ep}_{actPZ,min}$-values. This behavior will be discussed in more detail in the next section.

The J-integral values are collected in Tables 1 and 2. The values of $J^{ep}_{actPZ,max}$ lie approximately 6 % lower than the values of $J^{ep}_{PZ,max}$; the difference decreases to approximately 4 % with increasing crack extension. The difference almost disappears, if the active plastic zone merges with the back-face plasticity region so that general yielding (gy) conditions prevail. This happens for the values in Table 2 after $\Delta a = 4.6$ mm, see also Figs. 4c and 5c. The values of $J^{ep}_{PZ,min}$ are very close to

Table 2 Values of the incremental plasticity J-integrals around the crack tip plastic zone, J^{ep}_{PZ}, and around the active plastic zone, J^{ep}_{actPZ}, for large-scale yielding conditions

R	N	Δa (mm)	$J^{ep}_{PZ,max}$ (kJ/m^2)	$J^{ep}_{PZ,min}$	$J^{ep}_{actPZ,max}$	$J^{ep}_{actPZ,min}$	$\Delta^{J actPZ,max}_{J PZ,max}$ (%)	ΔJ^{ep}_{PZ} (kJ/m^2)	ΔJ^{ep}_{actPZ}	ΔJ^{exp}	$\Delta^{\Delta J actPZ}_{\Delta J PZ}$ (%)
0	1	0	10.56	0.000	10.56	0.008	0.00	–	–	10.42	–
0	2	0.2	10.83	0.008	15.27	−3.133	29.1	10.23	15.27	10.17	33.0
0	6	1	12.06	0.011	11.33	−0.575	−6.44	11.34	11.33	11.32	−0.09
0	11	2	14.02	0.019	13.30	−0.524	−5.41	13.01	13.30	13.06	2.18
0	16	3	16.81	0.045	16.19	−0.529	−3.83	15.12	16.19	15.24	6.61
0	21	4	21.40	0.143	21.25	−0.690	−0.71	18.04	21.25	18.12	15.1
0	*24*	*4.6*	*27.95*	*0.367*	*27.86*	*−1.015*	*−0.32*	*21.91*	*27.86*	*22.51*	*21.4*
0.5	1	0	10.56	0.000	10.56	2.832	0.00	–	–	10.42	–
0.5	2	0.2	10.81	2.832	14.85	3.520	27.2	2.578	3.910	2.568	34.1
0.5	6	1	12.00	3.135	10.72	1.743	−11.9	2.868	3.818	2.867	24.9
0.5	11	2	13.93	3.670	12.20	2.364	−14.2	3.300	3.823	3.321	13.7
0.5	16	3	16.69	4.511	15.05	3.111	−10.9	3.847	4.476	3.889	14.0
0.5	21	4	21.24	6.039	19.70	4.511	−7.82	4.628	5.357	4.695	13.6
0.5	*24*	*4.6*	*27.87*	*7.923*	*26.83*	*6.075*	*−3.88*	*6.073*	*7.371*	*6.419*	*17.6*
−1	1	0	10.56	0.000	10.56	5.2e−4	0.00	–	–	10.42	–
−1	2	0.2	10.84	5.2e−4	15.30	−3.608	29.1	10.69	15.30	10.57	30.1
−1	6	1	12.08	0.002	11.60	−0.484	−4.14	11.92	11.60	12.04	−2.76
−1	11	2	14.06	0.003	13.79	−0.454	−1.96	13.73	13.79	13.80	0.44
−1	16	3	16.90	0.004	17.04	−0.702	−0.82	16.45	17.04	16.63	3.46
−1	21	4	21.57	0.006	22.19	−1.166	−2.79	20.99	22.19	21.04	5.41
−1	*24*	*4.6*	*27.96*	*0.020*	*29.22*	*−1.680*	*−4.31*	*26.48*	*29.22*	*26.13*	*9.38*

The parameter R denotes the load ratio, N the load cycle number, and Δa the crack extension. The indices "max" and "min" denote maximum and minimum values during a load cycle. The values of the experimental cyclic J-integral ΔJ^{exp} are shown for comparison. General yielding conditions prevail for the rows marked in italics

zero for ssy-conditions (Table 1), whereas they reach several tenths of kJ/m^2 for lsy-conditions (Table 2), probably caused by irreversible elastic strain energy stored around the crack tip (Atkins and Mai 1986). The $J^{ep}_{actPZ,min}$-values are, in general, negative.

The incremental plasticity far-field J-integral J^{ep}_{far} equals J^{ep}_{PZ} for ssy-conditions. Due to the appearance of back-face plasticity, J^{ep}_{far} is lower than J^{ep}_{PZ} for lsy- and gy-conditions. With increasing crack length the difference between $J^{ep}_{far,max}$ and $J^{ep}_{PZ,max}$ increases from 0.5 % up to 33 %, due to the increase of the back-face plasticity region.

In all cases the J-integral for deformation plasticity J^{conv} equals the computational J-integral of ABAQUS, J^{VCE}. It is clear from Eq. (7) that $J^{conv}_{PZ} = J^{ep}_{PZ}$, unless gy-conditions appear. At the maximum load of every load cycle the deformation plasticity far-field J-integral comes close to the value around the plastic zone, $J^{conv}_{far,max} \approx J^{conv}_{PZ,max} = J^{ep}_{PZ,max}$, whereas at the minimum load of each load cycle, $J^{conv}_{far,min}$ strongly differs from the values of $J^{conv}_{PZ,min} = J^{ep}_{PZ,min}$. The reason has been already explained in detail in Ochensberger and Kolednik (2014), Sect. 4.2 therein: Artificial bulk configurational forces are induced in the back-face plasticity region since the conditions of proportional loading are violated during unloading. The deformation plasticity J-integral around the active plastic zone J^{conv}_{actPZ} shows an oscillating curve that continuously decreases with every load cycle, so that after a certain number of load cycles the values are negative even at maximum load.

Tables 1 and 2 collect also additional results of J^{ep}_{actPZ} and J^{ep}_{PZ} for load ratios $R = 0.5$ and -1 under ssy- and lsy-conditions. Especially for $R = 0.5$ and lsy-

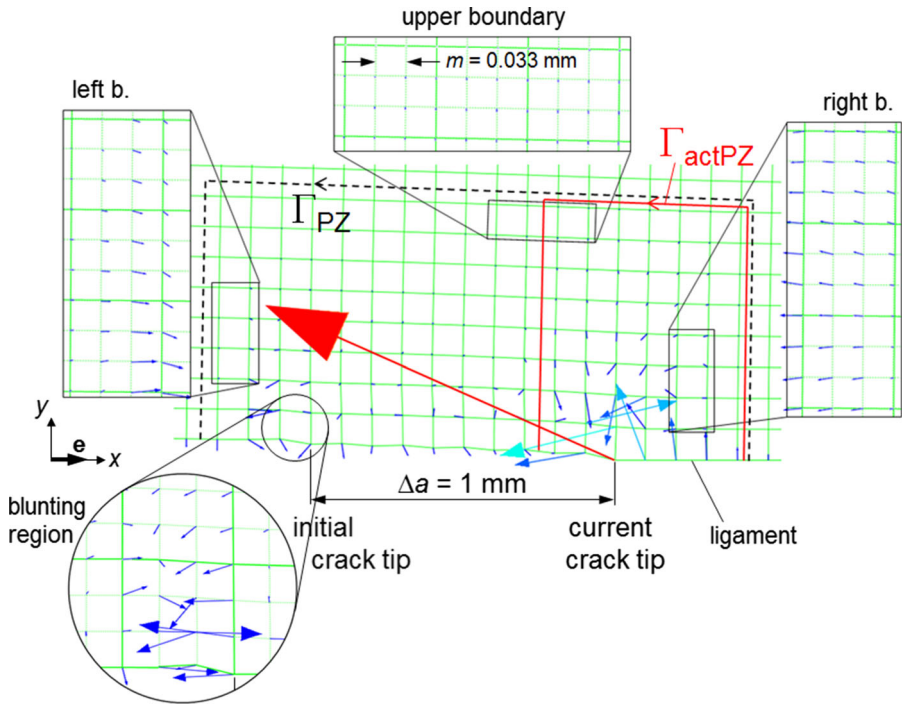

Fig. 6 Distribution of incremental plasticity bulk configurational force $\mathbf{f}^{\mathrm{ep}}$ in the entire crack tip plastic zone at a maximum load, $F_{\max} = 12.5\,\mathrm{kN}$, after a crack extension of $\Delta a = 1\,\mathrm{mm}$, compare Fig. 4a. Regions on the boundaries of the plastic zone and the bunting region of the initial crack tip are enlarged in detailed views; a finer mesh size of $m = 0.033\,\mathrm{mm}$ is used for a better visualization of the $\mathbf{f}^{\mathrm{ep}}$-vectors

conditions, the difference between the values at maximum load, $J^{\mathrm{ep}}_{\mathrm{actPZ,max}}$ and $J^{\mathrm{ep}}_{\mathrm{PZ,max}}$, can be significant.

4.2 Bulk configurational forces in the crack tip plastic zone

In order to explore the differences that appear in Fig. 5 between $J^{\mathrm{ep}}_{\mathrm{actPZ}}$ and $J^{\mathrm{ep}}_{\mathrm{PZ}}$, we analyze in this section the distribution of the bulk configurational force $\mathbf{f}^{\mathrm{ep}}$ in the crack tip plastic zone. For easier understanding, it is useful to transform Eq. (6) into small strain plasticity (Simha et al. 2008),

$$\mathbf{f}^{\mathrm{ep}} = \boldsymbol{\sigma} : \frac{\partial \boldsymbol{\varepsilon}^{\mathrm{p}}}{\partial \mathbf{x}}, \tag{13}$$

where $\boldsymbol{\sigma}$ denotes the Cauchy stress tensor and $\boldsymbol{\varepsilon}^{\mathrm{p}}$ the plastic part of the linear strain tensor $\boldsymbol{\varepsilon}$. Note that for crack and crack growth in x-direction, only the x-component of the configurational force $\mathbf{f}^{\mathrm{ep}}$-vector,

$$f_x^{\mathrm{ep}} = \sigma_{xx}\frac{\partial \varepsilon^{\mathrm{p}}_{xx}}{\partial x} + 2\sigma_{xy}\frac{\partial \varepsilon^{\mathrm{p}}_{xy}}{\partial x} + \sigma_{yy}\frac{\partial \varepsilon^{\mathrm{p}}_{yy}}{\partial x}, \tag{14}$$

contributes to the scalar J^{ep}-integral, see Eq. (5).

Figure 6 presents, for a load ratio $R = 0$, the distribution of the bulk configurational force $\mathbf{f}^{\mathrm{ep}}$ in the total crack tip plastic zone at maximum load $F_{\max} = 12.5\,\mathrm{kN}$ during the 6th load cycle, after 1 mm of crack growth. Important regions are enlarged in the detailed views where a finer mesh of $m = 0.033\,\mathrm{mm}$ is used to obtain a better visualization of the $\mathbf{f}^{\mathrm{ep}}$-vectors.[2]

On the left boundary of the crack tip plastic zone, $\mathbf{f}^{\mathrm{ep}}$-vectors appear with a positive f_x^{ep}-component, while f_x^{ep} is negative for $\mathbf{f}^{\mathrm{ep}}$-vectors on the right boundary. Along the upper boundary, $\mathbf{f}^{\mathrm{ep}}$-vectors emerge with x-components of almost zero; they only have a negative y-component f_y^{ep}. It is seen that in all cases the direction of $\mathbf{f}^{\mathrm{ep}}$-vectors clearly follows the gradient of the plastic strain, corresponding to Eq. (13); Fig. 4a includes schematically the directions of these $\mathbf{f}^{\mathrm{ep}}$-vectors. In the blunting region of the initial crack tip, the $\mathbf{f}^{\mathrm{ep}}$-vectors point to either direction, but the resulting configurational force, i.e. the sum of the x-components of all $\mathbf{f}^{\mathrm{ep}}$-vectors lying within this region, points into the negative x-direction.

The largest $\mathbf{f}^{\mathrm{ep}}$-vectors appear around the current crack tip, since there both stress and gradient of plastic strain are largest, Eq. (13). Due to symmetry, each

[2] For generating Fig. 6, the simulation was repeated with a FE-mesh size of $m = 0.033\,\mathrm{mm}$.

$\mathbf{f}^{\mathrm{ep}}$-vector that emerges from a node directly along the ligament in front of the current crack tip does have a "companion" $\mathbf{f}^{\mathrm{ep}}$-vector from the lower specimen half. The resulting $\mathbf{f}^{\mathrm{ep}}$-vector of both specimen halves has only a component in x-direction. This applies also for $\mathbf{f}^{\mathrm{ep}}_{\mathrm{tip}}$ which emerges from the current crack tip. For numerical reasons, $J^{\mathrm{ep}}_{\mathrm{tip}} = \mathbf{e} \cdot \left(-\mathbf{f}^{\mathrm{ep}}_{\mathrm{tip}}\right)$ has a finite value which depends on the FE-mesh size, see Kolednik et al. (2014). A decrease of the mesh size leads to a reduction of the magnitude of $J^{\mathrm{ep}}_{\mathrm{tip}}$ and yields finally $J^{\mathrm{ep}}_{\mathrm{tip}} = 0$. However, the values of $J^{\mathrm{ep}}_{\mathrm{actPZ}}$ (and $J^{\mathrm{ep}}_{\mathrm{PZ}}$) are not affected by a mesh refinement; Sect. 5.1 provides an example.

The variation of the difference between $J^{\mathrm{ep}}_{\mathrm{actPZ,max}}$ and $J^{\mathrm{ep}}_{\mathrm{PZ,max}}$ shown in Fig. 5a can be understood from Fig. 6 and Eq. (12): More and more bulk configurational forces $\mathbf{f}^{\mathrm{ep}}$ of the initial plastic zone become excluded from the integration contour Γ_{actPZ}, when it is shifted to the right during crack extension. First, the $\mathbf{f}^{\mathrm{ep}}$-vectors with positive f^{ep}_x-components from the left boundary are excluded, leading to the peak value of $J^{\mathrm{ep}}_{\mathrm{actPZ,max}}$ observed at $N = 2$. Next, the integration contour Γ_{actPZ} excludes the blunting region of the initial crack tip. Since the resulting $\mathbf{f}^{\mathrm{ep}}$ in this blunting region has a negative x-component, the value of $J^{\mathrm{ep}}_{\mathrm{actPZ,max}}$ drops below the value of $J^{\mathrm{ep}}_{\mathrm{PZ,max}}$. With further crack extension the difference between $J^{\mathrm{ep}}_{\mathrm{actPZ,max}}$ and $J^{\mathrm{ep}}_{\mathrm{PZ,max}}$ remains equal, since the excluded $\mathbf{f}^{\mathrm{ep}}$-vectors of the plastic wake have no x-component. It should be mentioned that a similar variation of $J^{\mathrm{ep}}_{\mathrm{actPZ}}$ is reported in Section 5.3 of Kolednik et al. (2014) for a growing crack under constant load.

For lsy-conditions, the difference between the values of $J^{\mathrm{ep}}_{\mathrm{actPZ,max}}$ and $J^{\mathrm{ep}}_{\mathrm{PZ,max}}$ decreases with increasing crack extension, because the right boundary of the active plastic zone, with $\mathbf{f}^{\mathrm{ep}}$-vectors in negative x-direction, increases. Finally, the difference nearly vanishes under gy-conditions.

The differences between $J^{\mathrm{ep}}_{\mathrm{actPZ,min}}$ and $J^{\mathrm{ep}}_{\mathrm{PZ,min}}$ at minimum load F_{min} can be explained analogously. Note that, due to the appearance of compressive stresses during unloading, the $\mathbf{f}^{\mathrm{ep}}$-vectors at F_{min} point into the opposite x-direction compared to the F_{max}-stage. This has been explained already in Ochensberger and Kolednik (2014), see also Sect. 2.3. It can be shown that negative $J^{\mathrm{ep}}_{\mathrm{actPZ,min}}$-values originate for $R \leq 0$ from these negative stresses; the relevance of these negative $J^{\mathrm{ep}}_{\mathrm{actPZ,min}}$-values will be discussed in the next section.

5 Driving force for fatigue crack growth

For a cyclically loaded, *stationary* crack, Ochensberger and Kolednik (2014) proposed the cyclic, incremental plasticity J-integral around the crack tip plastic zone, $\Delta J^{\mathrm{ep}}_{\mathrm{PZ}}$, as physically appropriate driving force parameter. Consequently, for a *growing* fatigue crack it is reasonable to adopt the cyclic, incremental plasticity J-integral around the *active* crack tip plastic zone, $\Delta J^{\mathrm{ep}}_{\mathrm{actPZ}}$, as the appropriate driving force parameter for fatigue crack growth. One argument is that only the active plastic zone travels with the crack tip during crack extension; the initial plastic zone and the plastic wake do not move. Another reason is that plasticity far from the current crack tip cannot be responsible for fatigue crack propagation that occurs due to cyclic plastic deformation at the current tip.

It seems obvious that $\Delta J^{\mathrm{ep}}_{\mathrm{actPZ}}$ should be evaluated, analogously to Eq. (9), by the relation,

$$\Delta J^{\mathrm{ep}}_{\mathrm{actPZ}} = J^{\mathrm{ep}}_{\mathrm{actPZ,max}} + J^{\mathrm{ep}}_{\mathrm{actPZ,min}} - 2\sqrt{J^{\mathrm{ep}}_{\mathrm{actPZ,max}} J^{\mathrm{ep}}_{\mathrm{actPZ,min}}}. \tag{15}$$

At this point we arrive at a dilemma when the incremental plasticity J-integral at minimum load, $J^{\mathrm{ep}}_{\mathrm{actPZ,min}}$, is negative, as shown in Tables 1 and 2 for load ratios $R = 0$ and $R = -1$, since this leads to a complex square root term. Therefore, it should be clarified in which form the negative values of $J^{\mathrm{ep}}_{\mathrm{actPZ}}$ in a load cycle deliver a contribution to the driving force for fatigue crack growth. We do this by studying the relation between the incremental plasticity J-integral J^{ep} and the crack tip opening displacement δ_{t}.

5.1 Incremental plasticity J-integral J^{ep} and crack tip opening displacement

Fatigue crack growth in ductile metals and alloys is driven by cyclic plasticity at the current crack tip (Laird 1967, 1979). The crucial role of crack tip plasticity was confirmed by experiments, e.g. Tanaka (1989), Krupp et al. (2002), and Pippan et al. (2010), where it was shown that the crack growth rate of a fatigue crack $\mathrm{d}a/\mathrm{d}N$ is a function of the cyclic crack tip opening displacement at the current crack tip, $\mathrm{d}a/\mathrm{d}N \propto \Delta\delta_{\mathrm{t}}$ with $\Delta\delta_{\mathrm{t}} = \delta_{\mathrm{t,max}} - \delta_{\mathrm{t,min}}$.

A correct numerical evaluation of the crack tip opening displacement δ_{t} during fatigue crack propa-

gation is difficult, since it requires a very fine FE-mesh. Experimental investigations using stereophotogrammetric measurements show that the crack tip opening displacement should be determined a distance behind the blunted crack tip, which corresponds to the width of the stretched zone (Kolednik and Stüwe 1985; Kolednik and Kutlesa 1989; Siegmund et al. 1990); a good approximation of this distance is for many materials given by 0.4 δ_t, see Kolednik and Stüwe (1987), Heerens et al. (1988). Therefore, δ_t should not be determined at a fixed distance behind the crack tip, since measurements at too large distances lead to an overestimate of δ_t, and vice versa. However, it is difficult to fulfill these requirements in practice. Dougherty et al. (1997) give a minimum element size m in order to determine accurate δ_t-values, $m/r_{pl} \leq 0.1$, where r_{pl} denotes the radius of the crack tip plastic zone. According to Solanki et al. (2003, 2004) the mesh size shall be further reduced by a factor $3 \div 4$. The relation $r_{pl} = \beta J E/\sigma_y^2$, with $\beta \approx 0.1$, yields for the maximum load of the 1st load cycle $r_{pl} \approx 0.59$ mm and $r_{pl} \approx 2.90$ mm for ssy- and lsy-conditions, respectively; this is roughly in agreement with Fig. 4a, b. The relation $J = k\,\sigma_y\,\delta_t$, with $J = J^{ep}_{PZ}$ and $k \approx 2$, yields values of the crack tip opening displacement, $\delta_t \approx 3.95$ µm and $\delta_t \approx 19.6$ µm, for ssy- and lsy-conditions, respectively. According to the criterion by Solanki et al. (1997), a mesh size of approximately $m \approx 4\delta_t$ would be sufficient for gaining accurate δ_t-values, which appears somewhat doubtful to us.

However, the computation of accurate δ_t-values is not very important for our purposes; our interest lies only in the correct reflection of crack tip opening and -closure behavior during the loading and unloading stages. Therefore, a mesh size of $m = 0.1$ mm should be sufficient for lsy-conditions; additional computations with smaller mesh size, $m = 10\,\mu$m, are conducted for ssy-conditions. The crack tip opening displacement is taken one element behind the current crack tip, as e.g. in Solanki et al. (2004).

Figure 7 shows the curves J^{ep}_{actPZ} versus δ_t during loading from F_{min} to F_{max} during the 6th load cycle, i.e. after a crack extension of $\Delta a = 1$ mm. The values for J^{ep}_{PZ} are included for comparison. The curves for ssy-conditions are plotted in Fig. 7a; Fig. 7b gives a detailed view of the region near the minimum load. Figure 7c, d present the curves for lsy-conditions. It is seen that $\delta_t = 0$ during the very initial loading stages. The curves suggest that the crack tip opening displacement δ_t does not start to increase before J^{ep}_{actPZ} becomes positive.

Thus, we state that negative values of J^{ep}_{actPZ} do not deliver a contribution to the fatigue crack growth rate, since the crack tip is closed during this stage. Moreover, from a thermodynamic view, a negative x-component of the $\mathbf{J}^{ep}_{actPZ}$-vector means that the crack feels a driving force for shortening its length. Therefore, the stage where the crack driving force is negative cannot deliver a contribution to the driving force for fatigue crack growth. For these reasons, we conclude that the negative values of J^{ep}_{actPZ} are not relevant for calculating the driving force for fatigue crack growth, and $\Delta J^{ep}_{actPZ} = J^{ep}_{actPZ,max}$ for $R = 0$.

It should be mentioned that the values of $J^{ep}_{actPZ,max}$ (and $J^{ep}_{PZ,max}$) are not affected by the decrease in mesh size m by a factor ten for ssy-conditions. For example, at maximum load we get $J^{ep}_{actPZ,max} = 2.279$ kJ/m^2 for $m = 10$ µm and $J^{ep}_{actPZ,max} = 2.280$ kJ/m^2 for $m = 0.1$ mm. On the contrary, the values of the crack tip opening displacement show a big variation: at maximum load we get $\delta_t = 3.11$ µm for $m = 10$ µm and $\delta_t = 4.65$ µm for $m = 0.1$ mm. This clearly demonstrates the advantage of the J-integral concept.

For negative load ratios $R < 0$ it can be also shown that negative $J^{ep}_{actPZ,min}$-values do not give a contribution to the cyclic J-integral ΔJ^{ep}_{actPZ}. Therefore, the driving force for fatigue crack growth is equal to the incremental plasticity J-integral around the active plastic zone at maximum load for zero-tension and tension-compression loading,

$$\Delta J^{ep}_{actPZ} = J^{ep}_{actPZ,max} \quad \text{for} \quad R \leq 0. \tag{16}$$

Note that the exact upper boundary for the validity of Eq. (16) has not been determined. For positive load ratios $R > 0$, the curves J^{ep}_{actPZ} and J^{ep}_{PZ} versus δ_t are almost linear and do not have a vertical part near F_{min}. Since both the $J^{ep}_{actPZ,min}$- and $\delta_{t,min}$-values are positive at minimum load, Eq. (15) must be used to evaluate ΔJ^{ep}_{actPZ}.

Table 1 lists ΔJ^{ep}_{actPZ}-values with increasing load cycle number N and crack extension Δa for load ratios, $R = 0, 0.5$ and -1, under ssy-conditions. The results for ΔJ^{ep}_{PZ}, Eq. (9), are collected for comparison. The difference between ΔJ^{ep}_{actPZ} and ΔJ^{ep}_{PZ} is of the order of 2 % for $R \leq 0$; on the contrary, ΔJ^{ep}_{actPZ} can even exceed ΔJ^{ep}_{PZ} by 13 % for $R = 0.5$. Table 2

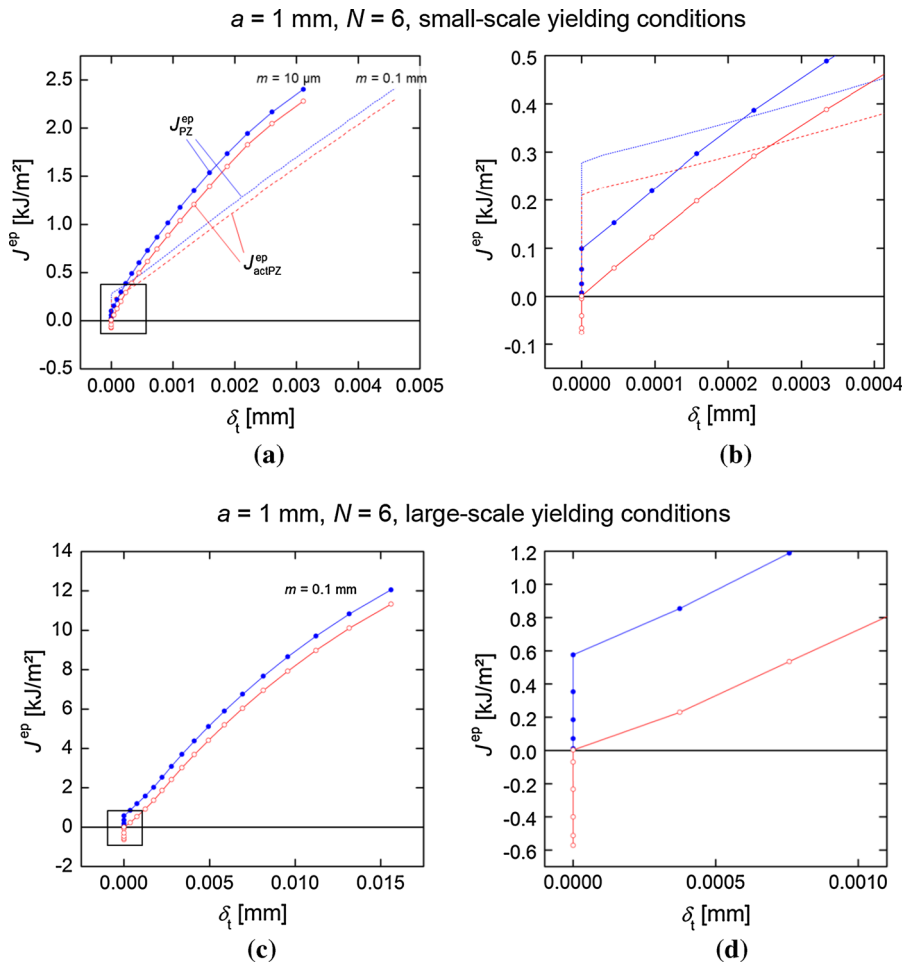

Fig. 7 Incremental plasticity J-integrals, J^{ep}_{actPZ} and J^{ep}_{PZ}, plotted against the crack tip opening displacement δ_t during re-loading after $\Delta a = 1$ mm crack extension. Values are depicted for **a** small-scale yielding, mesh sizes $m = 0.1$ mm and 10 µm; **c** large scale yielding, $m = 0.1$ mm. **b**, **d** Enlarged views of the beginnings of the loading sequences. The results suggest that loading stages where J^{ep}_{actPZ} is negative do not contribute to fatigue crack propagation, since δ_t is zero

lists corresponding values for lsy-conditions. Here, the difference between ΔJ^{ep}_{actPZ} and ΔJ^{ep}_{PZ} can become large for all load ratios. For $R = 0.5$, the values of $J^{ep}_{actPZ,min}$ are distinctively smaller than the $J^{ep}_{PZ,min}$-values which cause lower square root terms in Eq. (15) and, thus, significantly higher values of ΔJ^{ep}_{actPZ} compared to ΔJ^{ep}_{PZ}. Figure 8 presents, for a load ratio $R = 0$, the variations of ΔJ^{ep}_{actPZ} and ΔJ^{ep}_{PZ} with increasing crack extension. The variations of the cyclic crack tip opening displacement, $\Delta\delta_t = \delta_{t,max} - \delta_{t,min}$, with crack extension are shown for comparison.

The conclusion of this section is that the loading stages where $J^{ep}_{actPZ,min}$ becomes negative do not play a role for the calculation of the driving force for fatigue crack propagation. In the following section, the validity of the experimental cyclic J-integral ΔJ^{exp} proposed by Dowling and Begley (1976) shall be checked.

5.2 Comparison to the experimental cyclic J-integral ΔJ^{exp}

The experimental cyclic J-integral ΔJ^{exp} (Dowling and Begley 1976) is computed from the area ΔA below a single loading branch of the load–displacement ($F - v$) curve, Eq. (8). The ΔJ^{exp}-values for $R = 0$ are drawn into Fig. 8 and listed in Tables 1 and 2. It is seen that ΔJ^{exp} fits very well to the values of the cyclic, incremental plasticity J-integral ΔJ^{ep}_{PZ}. This corresponds to the findings reported in Sects. 2.2 and 2.3, and to Eq. (10). The experimental cyclic J-integral ΔJ^{exp} does not fit so well to ΔJ^{ep}_{actPZ}, although the error remains small for ssy-conditions. However, the error can reach 20 % for lsy-conditions. The values listed for $\Delta\frac{\Delta J^{actPZ}}{\Delta J^{PZ}}$ in Tables 1 and 2 are approximately equal to the relative difference between ΔJ^{ep}_{actPZ} and ΔJ^{exp}. Note that a small error of about 2 % has to be taken

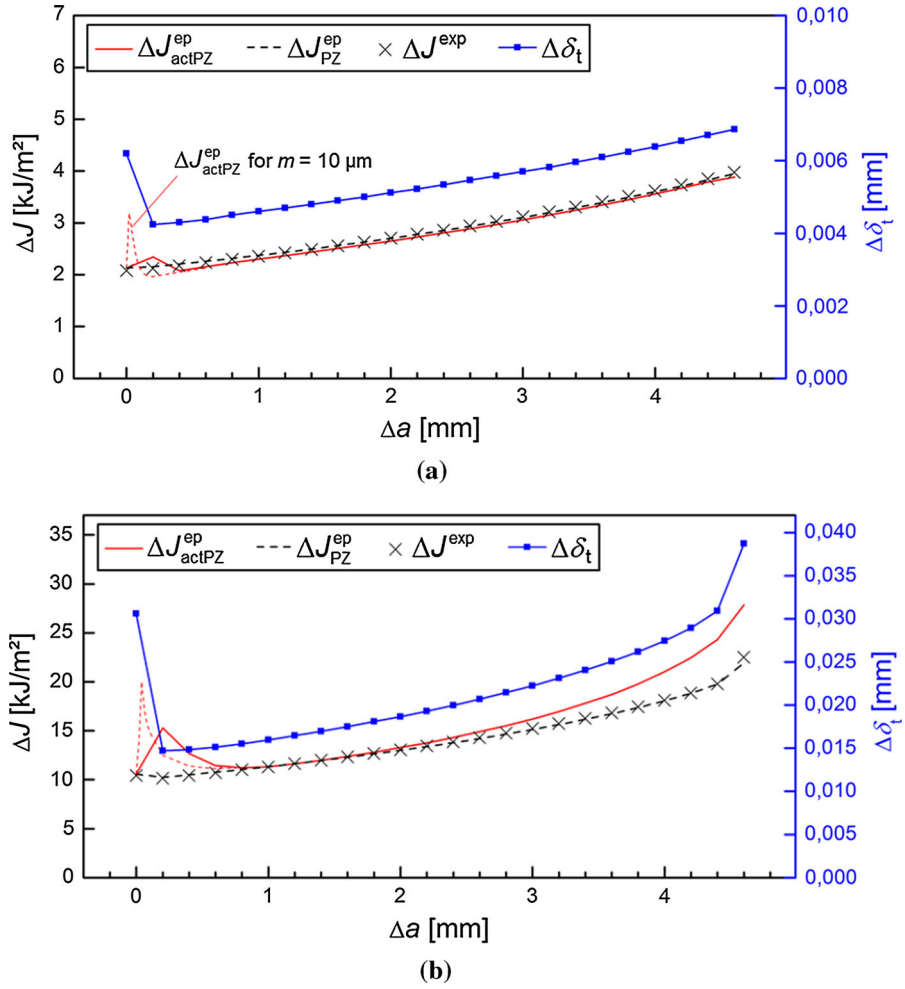

Fig. 8 Development of the cyclic, incremental plasticity cyclic J-integrals around the crack tip plastic zone, ΔJ^{ep}_{PZ}, and around the active plastic zone, ΔJ^{ep}_{actPZ}, with crack extension Δa. Values of the cyclic crack tip opening displacement $\Delta\delta_t$ and the experimental cyclic J-integral ΔJ^{exp} are drawn for comparison. **a** Small-scale yielding, **b** large-scale yielding conditions. The computations are made for a FE-mesh size of $m = 0.1$ mm; the first crack growth periods are re-calculated for a finer mesh size, $m = 10\,\mu$m, see dotted curves

into account in the evaluation of ΔJ^{exp}, which seems to result from an inaccuracy of the geometry factor η taken from ASTM E1820 (2005), compare the values listed for $N = 1$ in Tables 1 and 2.

Tables 1 and 2 collect also the ΔJ^{exp}-values for load ratios $R = 0.5$ and -1. For load ratios $R < 0$, in presence of crack closure, the values of ΔJ^{exp} depend on the correct determination of ΔA. According to Dowling and Begley (1976), the opening load F_{op} shall be determined from the compliance change that is visible as kink in the $F - v$-curve, Fig. 2b. Ochensberger and Kolednik (2014) showed for stationary cracks that this procedure tends to overestimate the driving force. Instead, ΔA should be determined as the area above the load $F_{J^{ep}_{PZ}=0}$, where the incremental plasticity J-integral around the crack tip plastic zone reaches its minimum value, $J^{ep}_{PZ,min} = 0$. The same procedure is used for the evaluation of the ΔJ^{exp}-values listed in Tables 1 and 2 for $R = -1$. The results show that ΔJ^{exp} fits very well toΔJ^{ep}_{PZ}, and Eq. (10) remains valid, unless gy-conditions prevail.

Crack closure does not occur for $R > 0$. It is seen that the misfit between ΔJ^{exp} and ΔJ^{ep}_{PZ} is small for various load ratios under ssy- and lsy-conditions, see Tables 1 and 2. In both cases the misfit slightly increases with increasing crack extension.

The validity of Eq. (10) becomes clear from the following: the condition $J^{ep}_{PZ} = J^{conv}_{PZ}$, Eq. (7), is fulfilled for cyclic loading conditions as long as the crack tip plastic zone is surrounded by elastically deformed material, see Sects. 2.2 and 2.3. The requirement for the validity of the condition $J^{conv}_{PZ} = J^{exp}$ is that a single loading cycle of a growing fatigue crack can be treated like a stationary crack under monotonic loading; only

then, the conventional J-integral and the experimental J-integral $J^{\exp}$ lead to the same results, see Rice et al. (1973), Kolednik (1991). This requirement is fulfilled during loading in each load cycle.

Table 1 shows that the experimental cyclic J-integral $\Delta J^{\exp}$ overestimates the driving force for fatigue crack growth $\Delta J^{\mathrm{ep}}_{\mathrm{actPZ}}$ by approximately 2 % for ssy-conditions and $R = 0$ and $R = -1$. On the contrary, $\Delta J^{\exp}$ considerably underestimates $\Delta J^{\mathrm{ep}}_{\mathrm{actPZ}}$ for $R = 0.5$, whereby the misfit decreases up to 12 % with increasing crack extension. For lsy-conditions, Table 2, $\Delta J^{\exp}$ underestimates $\Delta J^{\mathrm{ep}}_{\mathrm{actPZ}}$ for all load ratios. The misfit increases with crack extension to approximately 20 % for $R = 0$ and to 5 % for $R = -1$. For $R = 0.5$, the misfit of about 15 % is rather independent of crack extension. The reason for the high misfit under $R = 0.5$, even for ssy-conditions, is currently not fully understood by the authors, but it might be caused by the fact that proportional loading is fulfilled for each maximum load of a load cycle, which is required for the validity of $J^{\mathrm{ep}}_{\mathrm{PZ}} = J^{\exp}$, whereas this is not the case for the minimum load.

We can conclude this section by stating that the experimental cyclic J-integral does not exactly reflect the driving force for growing fatigue cracks in elastic–plastic materials, since it corresponds to the cyclic, incremental plasticity J-integral around the crack tip plastic zone, and not around the *active* plastic zone, $\Delta J^{\exp} \approx \Delta J^{\mathrm{ep}}_{\mathrm{PZ}} \neq \Delta J^{\mathrm{ep}}_{\mathrm{actPZ}}$. The difference between $\Delta J^{\exp}$ and $\Delta J^{\mathrm{ep}}_{\mathrm{actPZ}}$ can reach approximately 20 % for lsy-conditions.

6 The effect of a single tensile overload

In this section, a further test shall be conducted in order to check whether the cyclic, incremental plasticity J-integral for a contour around the *active* plastic zone, $\Delta J^{\mathrm{ep}}_{\mathrm{actPZ}}$, is the appropriate parameter for the characterization of the driving force for fatigue crack propagation, and not the cyclic J-integral for a contour around the plastic zone, $\Delta J^{\mathrm{ep}}_{\mathrm{PZ}}$. It is investigated whether $\Delta J^{\mathrm{ep}}_{\mathrm{actPZ}}$ is able to reflect the well-known overload effect: Crack growth retardation occurs, after a single tensile overload has been superimposed to cyclic loading with constant load amplitude. With further crack extension the crack growth rate gradually increases, reaching again the crack growth rate pertaining to the constant fatigue load somewhat after the active plastic zone has escaped from the plastic zone produced by the overload (Schijve 1960; Christensen 1959; von Euw et al. 1972; Suresh 1983; Fleck 1988; Skorupa 1998; Sadananda et al. 1999).

The fatigue crack growth rate $\mathrm{d}a/\mathrm{d}N$ in ductile metals and alloys is proportional to the cyclic crack tip opening displacement $\Delta\delta_{\mathrm{t}}$; this is so also after applying an overload. This fact was confirmed by experiments, e.g. Pippan et al. (2005) and Bichler and Pippan (1999; 2007), and by numerical studies, e.g. Tvergaard (2005). For example, Bichler and Pippan (2007) conducted ΔK-controlled fatigue tests under ssy-conditions with load ratio $R = 0.05$, using C(T)-specimens fabricated of ductile austenitic CrNi steel. The constant ΔK-fatigue history, with $\Delta K = 70\,\mathrm{MPa}\sqrt{\mathrm{m}}$, was interrupted by a single tensile overload with various overload ratios, $R_{\mathrm{OL}} = F_{\mathrm{OL}}/F_{\max} = 1.1 \div 2$. By analyzing fatigue striations (Zappfe and Worden 1951), which usually correlate with $\mathrm{d}a/\mathrm{d}N$ (Forsyth and Ryder 1960), and by conducting stereophotogrammetric measurements (Kolednik 1981) of the crack tip opening displacement δ_{t}, Bichler and Pippan (2007) demonstrated that the relation, $\mathrm{d}a/\mathrm{d}N \propto \Delta\delta_{\mathrm{t}}$, is valid also in the post-overload regime.

Our numerical test is conducted for zero-tension cyclic loading under ssy-conditions with applied maximum load, $F_{\max} = 12.5\,\mathrm{kN}$. A tensile overload, $F_{\mathrm{OL}} = 25\,\mathrm{kN}$, is applied in the fourth load cycle after $\Delta a = 0.6\,\mathrm{mm}$ crack extension (Fig. 3b); the overload ratio is $R_{\mathrm{OL}} = F_{\mathrm{OL}}/F_{\max} = 2$. Note that ssy-conditions still prevail during application of the overload, i.e. no back-face plasticity occurs. For our purpose, a FE-mesh size of $m = 0.1\,\mathrm{mm}$ was seen to be sufficient.

Figure 9 presents the variations of $\Delta J^{\mathrm{ep}}_{\mathrm{actPZ}}$, $\Delta J^{\mathrm{ep}}_{\mathrm{PZ}}$, the cyclic experimental J-integral $\Delta J^{\exp}$, and $\Delta\delta_{\mathrm{t}}$ as functions of the crack extension Δa. It is seen that $\Delta J^{\mathrm{ep}}_{\mathrm{actPZ}}$ varies analogously to $\Delta\delta_{\mathrm{t}}$ and clearly shows the retardation effect, whereas this is not the case for $\Delta J^{\mathrm{ep}}_{\mathrm{PZ}}$ and $\Delta J^{\exp}$.

The minimum value of $\Delta J^{\mathrm{ep}}_{\mathrm{actPZ}} = 0.269\mathrm{kJ/m}^2$ is reached after 0.4 mm of crack growth following the overload cycle, i.e. $\Delta a = 1$ mm total crack extension. This gives a reduction of about 88 % compared to the $\Delta J^{\mathrm{ep}}_{\mathrm{actPZ}}$-value at $\Delta a = 1\,\mathrm{mm}$ for a constant fatigue load, see Fig. 8a and Table 1. This value is in excellent agreement with the experimental results obtained by Bichler and Pippan (2007) from 25 mm thick C(T)-specimens (plane strain dominance), sub-

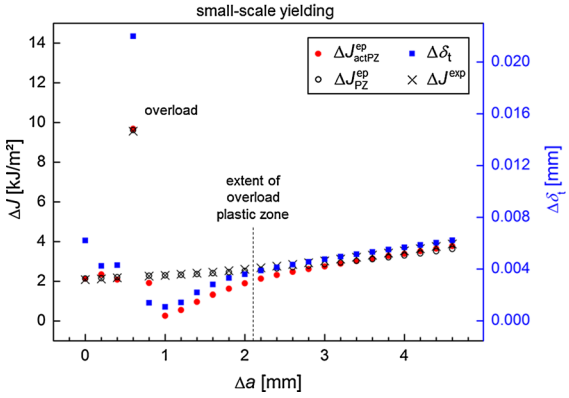

Fig. 9 Effect of a single tensile overload, applied during the 4th load cycle at $\Delta a = 0.6$ mm. The cyclic, incremental plasticity J-integrals around the crack tip plastic zone, ΔJ^{ep}_{PZ}, and around the active plastic zone, ΔJ^{ep}_{actPZ}, are plotted against crack extension Δa. Values of the cyclic crack tip opening displacement $\Delta\delta_t$ and the experimental cyclic J-integral ΔJ^{exp} are drawn for comparison. The parameter ΔJ^{ep}_{actPZ} correlates perfectly with $\Delta\delta_t$, exhibiting a crack growth retardation effect, whereas this is not the case for ΔJ^{ep}_{PZ} and ΔJ^{exp}

jected to $R_{OL} = 2$, where a maximal reduction in da/dN of about 84 % was observed after approximately 0.5 mm crack growth following the overload.

The overload case study has confirmed that the cyclic, incremental plasticity J-integral for a contour around the active plastic zone, ΔJ^{ep}_{actPZ}, is a physically appropriate driving force parameter for assessing the fatigue crack growth rate.

7 Computational aspects in the evaluation of ΔJ^{ep}_{actPZ}

In the following, a few issues regarding the computation of ΔJ^{ep}_{actPZ} shall be pointed out, which might be important for the practical application of the concept presented in the current paper.

The values of J^{ep}_{actPZ} are not affected of the used FE-mesh size, especially, in comparison to the expensive numerical effort that is necessary to obtain accurate results for the crack tip opening displacement δ_t, see Fig. 7a.

Provided that the active plastic zone has left the plastic zone of the initial crack tip, the magnitude of J^{ep}_{actPZ} is not significantly influenced by the magnitude of the integration contour Γ_{actPZ}. The reason is that the configurational forces in the plastic wake do not deliver a contribution to the value of J^{ep}_{actPZ}, see Sect. 4.2. Therefore, it is not important to find the exact shape of the active plastic zone (Fig. 4a).

However, one has to be careful during the initial stages of crack extension, especially, before the active plastic zone excludes the blunting region of the initial crack tip. In Sect. 4 we have shown that J^{ep}_{actPZ} at maximum load exhibits a peak value after the onset of crack extension; compare the $J^{ep}_{actPZ,max}$-values listed for $N = 2$ in Tables 1 and 2. Note that both position and magnitude of this peak value depend on the FE-mesh size m: A smaller mesh size gives a higher peak at smaller crack growth distance. The effect is shown in Fig. 8, for a reduction of m by a factor ten and a crack extension increment per load cycle of $\Delta(\Delta a) = 2m$. In this way, the finer FE-mesh is connected to a smaller crack extension increment per load cycle. Nevertheless, graphs similar to Fig. 7 can be also drawn for the first load cycles, showing that the crack tip is closed during the stages where J^{ep}_{actPZ} is negative and, thus, $\Delta J^{ep}_{actPZ} = J^{ep}_{actPZ,max}$, Eq. (16), is still valid and that ΔJ^{ep}_{actPZ} correlates to $\Delta\delta_t$.

The dependence of this peak value on the mesh size m is caused by the inhomogeneity of the plastic strain field around the crack tip, especially, near the blunted tip. A coarse mesh leads to a smoothing of stress and strain peaks and causes a reduction of the magnitude of the configurational force $\mathbf{f}^{ep}$, see Eq. (13).

Furthermore, it should be noted that additional FE-analyses are conducted where the crack extension in each load cycle occurs at maximum load. Basically, the results do not change compared to the procedure with crack extension at minimum load, and the same conclusions can be drawn as presented above.

8 Summary

The current paper discusses the physically correct evaluation of the driving force for fatigue crack propagation in elastic–plastic materials using the J-integral concept. Numerical investigations are conducted for a two-dimensional compact tension specimen with a long crack under cyclic Mode I loading. The crack extends by an increment after each load cycle at the minimum load. The maximum load is varied so that small- and large-scale yielding conditions prevail. Three different load ratios are considered, from pure tension to tension-compression loading. In general, maximum and mini-

mum load are held constant during crack extension; in addition, the effect of a single tensile overload is also studied.

The results of the analyses show that the cyclic, incremental plasticity J-integral $\Delta J^{\mathrm{ep}}_{\mathrm{actPZ}}$, which is computed for a contour around the *active* plastic zone of the growing crack, is physically appropriate to characterize the growth rate of fatigue cracks in elastic–plastic materials.

The experimental cyclic J-integral ΔJ^{exp}, proposed by Dowling and Begley (1976), measures the cyclic, incremental plasticity J-integral for a contour around the *total* plastic zone, $\Delta J^{\mathrm{ep}}_{\mathrm{PZ}}$; the contour includes also the plastic zone around the initial crack tip and the plastic wake. The experimental cyclic J-integral ΔJ^{exp} reflects the driving force of a stationary crack, i.e. it is valid for the first load cycle. After crack extension, the incremental plasticity J-integral around the total plastic zone $J^{\mathrm{ep}}_{\mathrm{PZ}}$ differs from that around the active plastic zone $J^{\mathrm{ep}}_{\mathrm{actPZ}}$. Therefore, $\Delta J^{\mathrm{ep}}_{\mathrm{PZ}} \neq \Delta J^{\mathrm{ep}}_{\mathrm{actPZ}}$, and the experimental cyclic J-integral ΔJ^{exp} is not fully appropriate to reflect the driving force for a *growing* fatigue crack.

The difference between $\Delta J^{\mathrm{ep}}_{\mathrm{actPZ}}$ and $\Delta J^{\mathrm{ep}}_{\mathrm{PZ}}$ is most clearly seen in the overload case, where $\Delta J^{\mathrm{ep}}_{\mathrm{actPZ}}$ is able to correctly reflect the well-known crack growth retardation effect, whereas $\Delta J^{\mathrm{ep}}_{\mathrm{PZ}}$ and ΔJ^{exp} would predict a constant crack growth rate.

Acknowledgments Financial support by the Austrian Federal Government and the Styrian Provincial Government within the research activities of the K2 Competence Center on "Integrated Research in Materials, Processing and Product Engineering", under the frame of the Austrian COMET Competence Center Programme, is gratefully acknowledged (strategic Project A4.20-WP3).

References

Anderson TL (1995) Fracture mechanics. CRC Press, Boca Raton, FL

ASTM E1820-05 (2005) Standard test method for measurement of fracture toughness. In: Annual book of ASTM standards, vol 03.01. ASTM International, West Conshohocken, PA, USA

Atkins AG, Mai YW (1986) Residual strain energy in elastoplastic adhesive and cohesive fracture. Int J Fract 30:203–221

Banks-Sills L, Volpert Y (1991) Application of the cyclic J-integral to fatigue crack propagation of Al 2024–T351. Eng Fract Mech 40:355–370

Bichler C, Pippan R (1999) Direct observation of the residual plastic deformation caused by a single overload. In: McClung RC, Newman JC Jr (eds) Advances in fatigue crack closure measurement and analysis, vol. 2, ASTM STP, West Conshohocken, PA. 1342:191–206

Bichler C, Pippan R (2007) Effect of single overloads in ductile metals: a reconsideration. Eng Fract Mech 74:1344–1359

Brocks W, Cornec A, Scheider I (2003) Computational aspects of nonlinear fracture mechanics. In: de Borst R, Mang HA (eds) Comprehensive structural integrity, numerical and computational methods, vol 3. Elsevier, New York, pp 127–209

Christensen RH (1959) Metal fatigue. McGraw-Hill, New York

Denzer R, Barth FJ, Steinmann P (2003) Studies in elastic fracture mechanics based on the material force method. Int J Numer Methods Eng 58:1817–1835

Dougherty JD, Padovan J, Srivatsan TS (1997) Fatigue crack propagation and closure behavior of modified 1071 steel: finite element study. Eng Fract Mech 56(2):189–212

Dowling NE, Begley JA (1976) Fatigue crack growth during gross plasticity and the J-integral. ASTM STP 590:82–103

Dowling NE (1976) Geometry effects and the J-integral approach to elastic–plastic fatigue crack growth. ASTM STP 601:19–32

Elber W (1970) Fatigue crack closure under cyclic tension. Eng Fract Mech 2:37–45

Elber W (1971) The significance of fatigue crack closure. ASTM STP 486:230–242

Eshelby JD (1951) The force on an elastic singularity. Philos Trans R Soc A 244:87–112

Eshelby JD (1970) Energy relations and the energy-momentum tensor in continuum mechanics. In: Kanninen M, Adler W, Rosenfield A, Jaffee R (eds) Inelastic behavior of solids. McGraw-Hill, New York, pp 77–115

ESIS P2-92 (1992) ESIS procedure for determining the fracture behavior of materials. European Structural Integrity Society, Delft

Fischer FD, Simha NK, Predan J, Schöngrundner R, Kolednik O (2012) On configurational forces at boundaries in fracture mechanics. Int J Fract 174:61–74

Fleck NA (1988) Influence of stress state on crack growth retardation. In: Fong JT, Fields RJ (eds) Basic questions in fatigue. ASTM STP 924, vol 1. ASTM:157–83

Forsyth PJE, Ryder DA (1960) Fatigue fracture. Aircr Eng 32:96–99

Gurtin ME (1995) The nature of configurational forces. Arch Ration Mech Anal 131:67–100

Gurtin ME (2000) Configurational forces as basic concepts of continuum physics. Springer, New York

Heerens J, Cornec A, Schwalbe K-H (1988) Results of a round robin on stretch zone width determination. Fatigue Fract Eng Mater Struct 11:19–29

Kienzler R, Herrmann G (2000) Mechanics in material space. Springer, Berlin

Kolednik O (1981) A contribution to stereophotogrammetry with the scanning electron microscope. Pract Metall 18:562–573

Kolednik O (1991) On the physical meaning of the J–Δa-curves. Eng Fract Mech 38:403–412

Kolednik O (1993) A simple model to explain the geometry dependence of the $J-a$-curves. Int J Fract 63:263–274

Kolednik O, Schöngrundner R, Fischer FD (2014) A new view on J-integrals in elastic–plastic materials. Int J Fract 187:77–107

Kolednik O, Stüwe HP (1985) The stereophotogrammetric determination of the critical crack tip opening displacement. Eng Fract Mech 21:145–155
Kolednik O, Stüwe HP (1987) A proposal for estimating the slope of the blunting line. Int J Fract 33:R63–R66
Kolednik O, Kutlesa P (1989) On the influence of specimen geometry on the critical crack-tip-opening displacement. Eng Fract Mech 33:215–223
Krupp U, Floer W, Lei J, Hu Y, Christ HJ, Schick A, Fritzen CP (2002) Mechanisms of short crack initiation and propagation in a beta-titanium alloy. Phil Mag A82:3321–3332
Kuna M (2008) Numerische Beanspruchungsanalyse von Rissen. FEM in der Bruchmechanik. Vieweg-Teubner, Wiesbaden
Laird C (1967) The influence of metallurgical structure on the mechanisms of fatigue crack propagation. ASTM STP 415:131–168
Laird C (1979) Mechanisms and theories of fatigue. ASM, Metals Park, OH, pp 149–203
Lamba HS (1975) The *J*-integral applied to cyclic loading. Eng Fract Mech 7:693–703
Lambert Y, Saillard P, Bathias C (1988) Application of the *J* concept to fatigue crack growth in large-scale yielding. ASTM STP 969:318–329
Maugin GA (1995) Material forces: concepts and applications. ASME J Appl Mech Rev 48:213–245
Metzger M, Seifert T, Schweizer C (2014) Does the cyclic *J*-integral describe the crack-tip opening displacement in the presence of crack closure? Eng Fract Mech. doi:10.1016/j.engfracmech.2014.07.017
Mueller R, Kolling S, Gross D (2002) On configurational forces in the context of the finite element method. Int J Numer Methods Eng 53:1557–1574
Mueller R, Gross D, Maugin GA (2004) Use of material forces in adaptive finite element methods. Comput Mech 33:421–434
Newman JC (1976) A finite element analysis of fatigue crack closure. ASTM STP 590:281–301
Nguyen TD, Govindjee S, Klein PA, Gao H (2005) A material force method for inelastic fracture mechanics. J Mech Phys Solids 53:91–121
Ochensberger W, Kolednik O (2014) A new basis for the application of the J-integral for cyclically loaded cracks in elastic-plastic materials. Int J Fract 189:77–101
Özenç K, Kaliske M, Lin G, Bhashyam G (2014) Evaluation of energy contributions in elasto-plastic fracture: a review of the configurational force approach. Eng Fract Mech 115:137–153
Ohji K, Ogura K, Yoshiji O (1975) Cyclic analysis of a propagating crack and its correlation with fatigue crack growth. Eng Fract Mech 7:457–464
Paris PC, Gomez MP, Anderson WP (1961) A rational analytic theory of fatigue. Trend Eng 13:9–14
Paris PC, Erdogan F (1963) A critical analysis of crack propagation laws. J Basic Eng 85:528–534
Parks DM (1977) The virtual crack extension method for nonlinear material behavior. Comput Methods Appl Mech Eng 12:353–364
Pippan R, Bichler C, Tabernig B, Weinhandl H (2005) Overloads in ductile and brittle materials. Fatigue Fract Eng Mater Struct 28:971–981
Pippan R, Zelger C, Gach E, Bichler C, Weinhandl H (2010) On the mechanism of fatigue crack propagation in ductile metallic materials. Fatigue Fract Eng Mater Struct 34:1–16
Rice JR (1968a) A path independent integral and the approximate analysis of strain concentration by notches and cracks. ASME J Appl Mech 35:379–386
Rice JR (1968b) Mathematical analysis in the mechanics of fracture. In: Liebowitz H (ed) Fracture—an advanced treatise, vol 2. Academic Press, New York, pp 191–311
Rice JR (1979) The mechanics of quasi-static crack growth. In: Kelly RE (ed) Proceedings of the eighth U.S. National congress of applied mechanics. ASME, New York, pp 191–216
Rice JR, Johnson MA (1970) The role of large crack tip geometry changes in plane strain fracture. In: Kanninen MF (ed) Inelastic behavior of solids. McGraw-Hill, New York, pp 641–672
Rice JR, Paris PC, Merkle JG (1973) Some further results of *J*-integral analysis and estimates. ASTM STP 536:231–245
Sadananda K, Vasudevan AK, Holtz RL, Lee EU (1999) Analysis of overload effects and related phenomena. Int J Fatigue 21:S233–S246
Schijve J (1960) Fatigue crack propagation in light alloy sheet material and structures. NRL report 195 MP National Aeronautical Research Institute, Amsterdam, Holland
Siegmund T, Kolednik O, Pippan R (1990) Direkte Messung der Rissspitzenverformung bei wechselnder Belastung. Z Metallkde 81 H.9:677–683
Simha NK, Fischer FD, Kolednik O, Chen CR (2003) Inhomogeneity effects on the crack driving force in elastic and elastic–plastic materials. J Mech Phys Solids 51:209–240
Simha NK, Fischer FD, Kolednik O, Predan J, Shan GX (2005) Crack tip shielding due to smooth and discontinuous material inhomogeneities. Int J Fract 135:73–93
Simha NK, Fischer FD, Shan GX, Chen CR, Kolednik O (2008) *J*-integral and crack driving force in elastic? Plastic materials. J Mech Phys Solids 56:2876–2895
Sistaninia M, Kolednik O (2014) Effect of a single soft interlayer on the crack driving force. Eng Fract Mech 130:21–41
Skorupa M (1998) Load interaction effects during fatigue crack growth under variable amplitude loading. A literature review. Part I: empirical trends. Fatigue Fract Eng Mater Struct 21:987–1006
Solanki K, Daniewicz SR, Newman JC Jr (2003) Finite element modeling of plasticity-induced crack closure with emphasis on geometry and mesh refinement effects. Eng Fract Mech 70:1475–1489
Solanki K, Daniewicz SR, Newman JC Jr (2004) Finite element analysis of plasticity-induced fatigue crack closure: an overview. Eng Fract Mech 71:149–171
Suresh S (1983) Micromechanisms of fatigue crack growth retardation following overloads. Eng Fract Mech 18:577–593
Suresh S (1998) Fatigue of materials, 2nd edn. Cambridge University Press, Cambridge
Tanaka K (1983) The cyclic *J*-integral as a criterion for fatigue crack growth. Int J Fract 22:91–104
Tanaka K (1989) Mechanics and micromechanics of fatigue crack propagation. ASTM STP 1020:151–183
Turner CE, Kolednik O (1994) Application of energy dissipation rate arguments to stable crack growth. Fatigue Fract Eng Mater Struct 17:1109–1127

Tvergaard V (2005) Overload effects in fatigue crack growth by crack-tip blunting. Int J Fatigue 27:1389–1397

von Euw EFJ, Hertzberg RW, Roberts R (1972) Delay effects in fatigue crack propagation. In: Stress analysis and growth of cracks, ASTM STP 513, part I. Philadelphia ASTM:230–259

Wüthrich C (1982) The extension of the J-integral concept to fatigue cracks. Int J Fract 20:R35–R37

Zappfe CA, Worden CO (1951) Fractographic registrations of fatigue. Trans Am Soc Met 43:958–969